NASA Technical Memorandum 88235

Vortex Simulation of Forced Mixing Layers

Osamu Inoue and Anthony Leonard

June 1986

NASA
National Aeronautics and
Space Administration

NASA Technical Memorandum 88235

Vortex Simulation of Forced Mixing Layers

Osamu Inoue,
Anthony Leonard, Ames Research Center, Moffett Field, California

June 1986

National Aeronautics and
Space Administration

Ames Research Center
Moffett Field, California 94035

This Page Intentionally Left Blank

NOMENCLATURE

A	Amplitude of forced periodic disturbance
b	Mixing layer thickness, $b = y_{0.95} - y_{0.1}$
f	Frequency of forced periodic disturbance
f_p	Predominant frequency
L	Half width of a duct
l	Distance between two neiboring vortices upstream of the origin
N_{up}	Number of vortices upstream of the origin
r	Velocity ratio, $r = U_2/U_1$
t	Time
$U_1,\ U_2$	Freestream velocities ($U_1 > U_2$)
U_c	Convection velocity, $U_c = (U_1 + U_2)/2$
u	Velocity in x direction
v	Velocity in y direction
x	Streamwise coordinate
x_{max}	Downstream distance beyond which vortices are deleted
x_{test}	Downstream distance of the test section
y	Normal coordinate
z	Complex representation of (x, y), $z = x+iy$
Γ	Circulation
δt	Time step
δ_w	Vorticity thickness
ΔU	Velocity difference, $\Delta U = U_1 - U_2$
ϵ	Core radius
θ	Momentum thickness

θ_e Energy thickness

λ Modified velocity ratio, $\lambda = (U_1 - U_2)/(U_1 + U_2)$

Subscript

n n-th vortex

f forced disturbance

Vortex Simulation of Forced Mixing Layers

OSAMU INOUE[1] AND ANTHONY LEONARD[2]

NASA Ames Research Center
Moffett Field, CA 94035

ABSTRACT

Two-dimensional, spatially growing, turbulent mixing layers are simulated numerically by a vortex method and the results are compared with those determined experimentally. The effects of artificial forcing on flow development are also studied. Many of the flow features which have been observed experimentally are reproduced, and good quantitative agreements between experiments and computations are obtained.

INTRODUCTION

Vortical flow structures of turbulent mixing layers are now well recognized, and the vortex method has been applied to simulate these vortical flows (Saffman and Baker, 1979; Aref, 1983; Leonard,1985). Though time-developing flows have been frequently treated with computations because of their relative simplicity, simulation of spatially growing mixing layers is preferably accomplished by quantitative comparison with experiments.

Ashurst (1979) simulated a spatially growing mixing layer for the first time by a vortex method. He showed that vortex pairing plays an important role in the development of a turbulent mixing layer, which is consistent with experimental observations. Mansour (1985) simulated a spatially growing mixing layer using a

[1]NRC Research Associate. On leave from Institute of Space and Astronautical Science, Japan.
[2]Present address: Graduate Aeronautical Laboratories, California Institute of Technology, Pasadena, CA 91125.

hybrid numerical scheme. which is a combination of a Lagrangian vortex method with an Eulerian finite-difference method. He simulated mixing layers with and without forcing. and obtained the entrainment ratio numerically for the first time. One of the authors, Inoue (1985a,b), also simulated a spatially growing mixing layer with and without forcing by a vortex method. He showed by using passive markers that entrainm nt is an important mechanism for growth of the mixing layer.

In spite of such contributions, it is not yet clear how well two-dimensional (2D) vortex methods simulate turbulent mixing layers, the reason being the small number of calculated data which are quantitatively comparable with experimental data. One of the goals of this study was to add new data to our knowledge concerning the applicability of a vortex method to simulate mixing layers. We also wanted to increase our understanding of a turbulent mixing layer. The numerical method we used is an adaptation of that used by Inoue (1985b).

First, we take the effect of walls into consideration because many of the experiments have been performed in a wind tunnel. It is known that an infinite number of rows of image vortices satisfy the wall condition that normal velocity vanishes on the wall. In actual computations, this method is very expensive. We consider three simplified treatments of the walls. In Model A, two rows of vortices are located at image positions with respect to the upper and lower walls. These image vortices have the opposite sense of circulation and half the strength of the real vortices. This ensures that the total circulation of the flow field remains zero. In Model B, two rows of vortices as in Model A have the opposite sign to and the strength of half of the real vortices, but are aligned with a fixed distance l between each of the neighboring vortices, respectively, on a line at $y = 2L$ and $y = -2L$, where L is the distance between the splitter plate and a wall. The number of vortices on the lines is adjusted at each time so that total circulation of the flow field vanishes. In Model C, two vortex sheets are used instead of two rows of discrete vortices in Model B and

the length of the vortex sheets is adjusted so that total circulation vanishes. Strictly speaking, the normal velocities on "our walls" do not satisfy the wall condition in either case. However, the normal velocities on our walls are very small when the distance between the walls is sufficiently larger than the mixing layer thickness.

Second, we delete vortices from the computation when they are sufficiently far downstream. This treatment ensures that the maximum number of discrete vortices in the computational domain is within a certain limit, and thus allows a calculation to be made for a period long enough that statistics can be measured. In most of the cases to be presented, velocities were averaged over $200 \leq t \leq 1,400$ in our time units, which is 12 times longer than the averaging time used by Inoue (1985b), that is $120 \leq t \leq 220$. In our longest calculation, velocities were averaged over $200 \leq t \leq 11,000$. The average number of vortices existing in the computational domain was about 2600.

Increasing attention has been given to forced mixing layers, because forcing may provide possible turbulence control (Ho and Huerre, 1984). Zaman and Hussain (1980) imposed disturbances using sound from a loudspeaker. The results showed that reduction of turbulence intensity can occur under certain conditions of forcing disturbances. Ho and Huang (1982) imposed disturbances on a flow by controlling flow rate. Their results showed that the spreading of a mixing layer can be efficiently manipulated at very low forcing frequency, if the mixing layer is perturbed near a subharmonic of the response frequency. Oster and Wygnanski (1982) generated disturbances using a small vibrating flap installed downstream of the trailing edge of a splitter plate. They found that the growth of the mixing layer depends both on the amplitude and the frequency of the forced disturbances. All these experiments showed that the flow features of a mixing layer strongly depend on the forced disturbances. In this paper, the effect of forcing on the development of a mixing layer is also examined. There are a variety of methods by which forcing is applied

numerically (Inoue, 1985a; Mansour, 1985; McInville, Gatski, and Hassan, 1985). One of the simplest methods is to impose velocity disturbances of a sinusoidal form at the end of a splitter plate (Inoue,1985a). This is the method adopted for this study.

MATHEMATICAL FORMULATION AND NUMERICAL PROCEDURE

The flow model and numerical method we considered are similar to those used in previous studies (Inoue, 1985a,b), except that the effect of walls is taken into consideration. First, we consider an unbounded flow produced by an infinite row of discrete vortices with the same sign and the same strength which are moving along the x-axis with a constant velocity. Let the circulation of each vortex be denoted by Γ, the fixed distance between the two neighboring vortices by l, the constant velocity of the vortices by U_c, and the upper- and lower-side velocities of the flow far from the x-axis by U_1 and U_2, respectively. Then the following relations are satisfied.

$$\Gamma = \Delta U \cdot l \tag{1}$$

$$\Delta U = U_1 - U_2 \tag{2}$$

$$U_c = (U_1 + U_2)/2 \tag{3}$$

Next, let us suppose that at an initial instance, $t = 0$, vortices on the right ($x > 0$) are suddenly removed. At all subsequent times the vortices on the left ($x < 0$) are assumed to move along the x-axis with the convection velocity U_c. After reaching the origin ($x = 0$), each vortex with $x > 0$ is assumed to move under the influence of the potential field induced by individual vortices including the upstream ($x < 0$) vortices, in addition to the contribution of the convection velocity. Our main interest lies in the motion of the discrete vortices on the right side. To accurately simulate a flow produced in a wind tunnel, the effect of walls which bound the mixing layer

at $y = \pm L$ should be taken into consideration. An infinite number of rows of image vortices are necessary to satisfy the wall condition that the normal velocity vanish on the wall. In actual computations the evaluation of the effect of the infinite number of rows of image vortices is very time-consuming. Furthermore, we plan to extend this calculation to three dimensions, in which case an image system with an infinite number of vortex filaments is not feasible. In this paper, the effect of walls is approximated by two rows of vortices only (Models A and B) or by two vortex sheets (Model C). These vortices have circulation $-\Gamma/2$ and are located either at the image positions with respect to the upper and the lower walls (Model A, see figure 1) or on the lines at $y = \pm 2L$ with the distance l between each neighboring vortices (Model B). In Model C, vortex sheets are located at $y = \pm 2L$. Note that the strength of these vortices or the vortex sheets is prescribed such that total vorticity of the flow field is zero. Strictly speaking, normal velocities on our walls do not vanish. As will be seen, normal velocity on the walls is very small when the distance between the upper and lower walls is sufficiently larger than the mixing layer thickness. In Model A and Model B the complex velocity potential, f, which governs the flow development for N vortices, is given by

$$f = U_c z + i \sum_{n=1}^{N} \frac{\Gamma}{2\pi} log(z - z_n) - i \sum_{n=1}^{N} \frac{\Gamma}{4\pi} log(z - z_{u,n}) - i \sum_{n=1}^{N} \frac{\Gamma}{4\pi} log(z - z_{l,n}) \quad (4)$$

where $z = x + iy$, and the subscripts u and l denote the upper- and lower-image vortices, respectively. The velocity components u in the x-direction and v in the y-direction are given by

$$u - iv = \frac{\partial f}{\partial z}$$

In Model C, the velocity components are given by

$$u - iv = U_c + i \sum_{n=1}^{N} \frac{\Gamma}{2\pi} \frac{1}{z - z_n} + i \frac{\Gamma}{4\pi l} log(\frac{z_{max,u} - z}{z_{up,u} - z}) + i \frac{\Gamma}{4\pi l} log(\frac{z_{max,l} - z}{z_{up,l} - z}) \quad (5)$$

where z_{max} and z_{up} denote the downstream and upstream positions of the vortex sheets, respectively. The time development of an individual vortex is determined

from the relation

$$\frac{dx_n}{dt} = u_n, \qquad \frac{dy_n}{dt} = v_n$$

As is well known, the numerical algorithm employed here requires evaluation of N^2 order terms per time step and therefore is very time consuming for large N. To save computation time, we assume a test section in which reliable results are expected to be defined as $0 < x < x_{test}$, and vortices far downstream ($x \geq x_{max} > x_{test}$) of the test section are deleted.

In cases where forcing is applied, each new discrete vortex that appears at the origin is assigned the velocity

$$u = U_c, \qquad v = v_f(t)$$

in addition to the velocity induced by individual discrete vortices (Inoue, 1985a). Periodic disturbances of the form

$$v_f(t) = Asin(2\pi ft)$$

are assumed.

In this simulation, the first-order Euler scheme is employed for time integration. After a number of preliminary tests, the simulation parameters were prescribed as follows

$$U_c = 3.2, \quad \delta t = 0.1, \quad x_{test} = 250.0$$

$$r = U_2/U_1 = 0.3, \ \ 0.46, \ \ 0.6 \tag{6}$$

$$f = 0.0, \ 0.08, \ 0.16, \ 0.32, \ 0.64$$

$$A = 0.0, \ 0.01U_c, \ 0.1U_c, \ 0.5U_c, \ U_c$$

The above velocity ratios were selected by taking into consideration the experiments of Oster and Wygnanski (1982) and Mehta and Westphal (1985). The distance between two neighbouring vortices upstream of the origin was prescribed to be

$l = U_c \delta t (=0.32)$, and therefore vortices are shed one by one at every time-step δt from the origin. In this calculation as in the previous ones (Inoue, 1985a,b), the following core function was used.

$$u \propto \sum_{n=1}^{N} \frac{y - y_n}{(x - x_n)^2 + (y - y_n)^2 + \epsilon^2} \tag{7}$$

Four additional parameters must be fixed in addition to those simulation parameters described earlier in (6). These are the core radius ϵ, downstream distance, x_{max}, beyond which vortices are deleted, half width of a duct L, and number of vortices N_{up} upstream of the origin. The effects of these parameters on flow features are slight. The difference of calculated results among Model A, Model B and Model C is also very small. Therefore, most of the calculations were performed using Model A with $\epsilon = 0.6l$, $x_{max} = 500.0$, $L = 50.0$, and $N_{up} = 1000$.

RESULTS AND DISCUSSION

Mixing Layers Without Forcing

Motions of discrete vortices at the initial stage of time development are presented in figure 2. At the initial stage, vortices leaving the origin roll up into concentrated swirls, as shown in figure 2(a). These swirls grow with time, and move into the lower-speed flow region,as shown in figures 2(b) and 2(c). In contrast to unbounded mixing layers, further movement of the swirls toward the lower-speed flow side is prevented by the image vortices, and the swirls are convected downstream along the wall with a velocity approximately equal to U_c (figures 2(d) and 2(e)). After sufficient time, it appears that the state of the mixing layer in the test section is independent of the effect of the initial roll up. In our calculations, a quasi-steady state of the mixing layer is achieved in the test section, $0 \leq x \leq 250$, after approximately $t = 140$ (figure 2(f)). Measurements of velocity fields are started at $t = 200$ when the initial swirls

have passed the location $x = 500$ (figure 3). This downstream location is prescribed in most cases of this calculation as the maximum value, x_{max}, beyond which vortices are deleted from the computation. Velocities are measured at twelve stations of x from 20 to 240, and 51 points of y from -20 to 20 at each x-station. The mean flow quantities and turbulent statistics are obtained by averaging instantaneous values over the period $200 \leq t \leq 1,400$ in most cases. A much longer calculation performed over $200 \leq t \leq 11,000$ confirms that the shorter averaging time is enough to obtain accurate values of lower-order statistics like the Reynolds stress $(-\overline{u'v'})$. Figures 4-7 are graphs of mean flow quantities obtained in these calculations. The actual data are shown in table 1 (case 1 and case 2). Examples of flows in a quasi-steady state are presented in figure 8 for three different velocity ratios, $r = 0.6$, 0.46, and 0.3.

For this study, we measured several characteristic thicknesses of the mixing layer. These are presented in figures 9 and 10 for $r = 0.6$. The various thicknesses are momentum (θ), mixing layer (b), vorticity (δ_w), and energy (θ_e). These have been calculated as shown below.

$$\theta = \int \frac{U-U_2}{U_1-U_2} \{1 - \frac{U-U_2}{U_1-U_2}\} dy$$

$$b = y_{0.95} - y_{0.1}$$

$$\delta_w = \frac{\Delta U}{\left(\frac{\partial U}{\partial y}\right)_{max}}$$

$$\theta_e = \int \frac{U-U_2}{U_1-U_2} \{1 - \left(\frac{U-U_2}{U_1-U_2}\right)^2\} dy$$

All thicknesses presented show linear growth for $x > 60$. In the figures, for example, the symbol $y_{0.5}$ denotes the location at which $U = U_2 + 0.5(U_1 - U_2)$. The locus of $y_{0.5}$ is also linear for $x > 60$, but the values are negative as the location of $y_{0.5}$ moves toward the lower speed flow region (Oster and Wygnanski, 1982).

Time averaged profiles of the mean velocity, fluctuation velocities, the Reynolds stress, and third-order moments are presented in figures 11-14 for $r = 0.6$ of the longer averaging time. The velocities were made dimensionless by ΔU. The modified

mean velocity, $\bar{u} = (U - U_2)/\Delta U$, is plotted in figure 11, instead of the mean velocity, U. The coordinate η is defined as $(y - y_{0.5})/\theta$. All the mean quantities plotted in figure 11 are similar in shape. We observed that some features of the calculated results differed from those of the experimental results. First of all the maximum value of *r.m.s.* u' is smaller than that of *r.m.s.* v' (figure 12), which contradicts experimental results at high Reynolds number. Second, the profile of *r.m.s.* u' is deformed in shape if it is compared with the profiles obtained experimentally (for example, Oster and Wygnanski, 1982). The profile of *r.m.s.* v' is smooth and quite similar in shape to experimental results. Third, the profiles of both $\overline{u'^3}$ and $\overline{u'v'^2}$ in figure 14 show bumps near the boundaries of a mixing layer, which have not been observed in the experimentally determined profiles. There is some evidence that the discrepancy between our calculation and experimental value of the relative magnitude between *r.m.s.* u' and *r.m.s.* v' and the deformed shape of *r.m.s.* u' may be a result of the three dimensionality existing in actual flows. We discuss this point later in relation to the effect of forcing. Both Ashurst(1979) and Mansour (1985) also found similar results, that is, a deformed profile of *r.m.s.* u' and *r.m.s.* u' values less than *r.m.s.* v'.

The effects of velocity ratio r on flow features are plotted in figures 15-20. Figures 15 and 16 show that the mixing layer grows more rapidly with decreasing r. In these figures the results of the longer calculation are also plotted for $r = 0.6$. One can see that the difference of mixing layer growth caused by different averaging times is slight (see table 1). In figures 17-20, the profiles at five stations in the x-direction, x=120, 140, 160, 180 and 200, are plotted with the same symbol for each velocity ratio. Figure 17 suggests that the similarity profile of the modified mean velocity $\bar{u}$ is independent of the velocity ratio r. The other quantities presented in figures 17-20 show that the peak values of the similarity profiles are approximately independent of r, at least for the first- and second-order moments. Note that the maximum value

of $r.m.s.\ u'$ in the experiment of Oster and Wygnanski (1982) was approximately a constant independent of the velocity ratio.

A comparison of the calculated data (Model A with $L = 50.0$) with the experimental data is presented in table 2. In the table the mixing layer thickness b is defined, according to Oster and Wygnanski (1982), as $b = y_{0.95} - y_{0.1}$ for both $r = 0.6$ and $r = 0.3$ while according to Mehta and Westphal (1985) as $b = y_{0.9} - y_{0.1}$ only for $r = 0.46$. The maximum values of $r.m.s.\ u'$, $r.m.s.\ v'$ and of the Reynolds stress, $-\overline{u'v'}$, are obtained from their respective similarity profiles. The agreement between the calculated and experimental is good, except for the peak values of $r.m.s.\ v'$ which are twice as high as the experimental values. It is important to realize that Mehta and Westphal (1985) performed their experiment without walls and that our calculation is in good agreement with their results. This agreement is achieved even with the wall effect of our calculation.

A number of tests were performed to study effects of parameters on flow features. The parameters tested are core radius (ϵ), half width of a duct (L), the downstream distance beyond which vortices are deleted (x_{max}), and the number of vortices which are aligned upstream of the origin (N_{up}). Some of the results are presented in table 1 for $r = 0.6$. The mean quantities are obtained by averaging instantaneous values over the shorter time period except for Case 1 when the longer averaging time was used. The computational condition of Case 1 is identical to Case 2 except for the averaging time. Comparison of Case 1 with Case 2 indicates that the shorter averaging time is sufficient in determining the low order moments as presented in table 1. This conclusion is supported by figures 4-7. The effect of the parameters on the mean flow quantities is slight, except for a very narrow wall width (Case 7 in table 1) where the Reynolds stress $-\overline{u'v'}$ did not show similarity for the shorter averaging time. The effect of L on the mixing layer thicknesses is plotted in figures 21 and 22 for $r = 0.6$. Except for the case of the narrow duct width ($L = 30.0$), the effect of

L on the mixing layer thicknesses is negligible. However, the momentum thickness, θ, shortly downstream of the splitter plate shows a small difference between the cases of $L = 50.0$ and $L = 70.0$. The peak value of $r.m.s.\ u'$ is smaller than that of $r.m.s.\ v'$ in every case, even in Case 8 where the effect of walls is not considered. The difference between this result and the result of Inoue (1985b), $r.m.s.\ u' > r.m.s.\ v'$, may be caused by insufficient averaging time in the calculation, $120 \leq t \leq 220$. The results obtained using Model B and Model C are presented in table 1. The difference between Case 11 and Case 12 and between Case 13 and Case 14 is the wall width L. The difference between the calculated results of the three models used is small. Mixing layer thicknesses and statistical quantities for all three models with $L = 50.0$ are shown in figures 23-28. In figures 25 to 28, only the values at $x = 200.0$ are plotted as typical for Model A, while for Models B and C, the values from $x = 120.0$ to 200.0 are plotted with the same symbol.

The effect of parameters on the normal velocity V on our walls is summarized in figures 29 and 30. The velocity V is normalized by ΔU. Figure 29(a) shows that when L is fixed the magnitude of the normal velocity V on the walls becomes larger with decreasing velocity ratio r. Figure 29(b) shows that when r is fixed, the magnitude of V on the walls has a tendency to become larger with increasing L. This is ironical because the calculated results show better agreement with experiments with a large L than with a small L (see table 1). With a very large L, the effect of walls is negligible and in such cases the linearity of the centerline $y_{0.5}$ of the mixing layer may not hold. In fact, $y_{0.5}$ does not show linearity without walls (Case 8 in table 1). The normal velocity V on the walls shows very little variation among the three models as confirmed by the same values of both r and L (see figure 30). The velocity V on the walls was less than 1.6 percent of ΔU and the $r.m.s.\ v'$ on the walls was less than 0.5 percent of ΔU in our calculation. This result, coupled with good agreement between experimental and calculated values in Table 2, indicates

that the wall models adopted here provide no practical problems.

Forced Mixing Layers

The effects of periodic forcing on the flow features were investigated using Model A under the conditions of $r = 0.6$, $U_c = 3.2$, $\delta t = 0.1$, $\epsilon = 0.6l$, $x_{max} = 500$, $L = 50$, and $N_{up} = 1000$. In the experiments of Oster and Wygnanski (1982) the predominant frequency f_p of the unforced mixing layer with $r = 0.6$ satisfied the following relation near the trailing edge

$$\frac{f_p\,\theta_i}{U_1 + U_2} \approx 0.02 \tag{11}$$

This relation can also be obtained by stability analysis (Michalke, 1965). In our calculation, $U_1 + U_2 = 2U_c = 6.4$, and the momentum thickness, θ_i, obtained near the start of linear growth of the unforced mixing layer is approximately equal to 0.4, as seen in figure 9. Therefore the predominant frequency, f_p, may be determined from the above relation as $f_p \approx 0.32$.

The dependence of the mixing layer thicknesses on forcing frequency is presented in figures 31 and 32. The difference among flows caused by the variation of forcing frequency is shown in figure 33 with $t = 1000.0$. For unforced cases mixing layers grow linearly with x, as seen in figures 31 and 32. For a low frequency forced flow ($f = 0.16$), all mixing layer thicknesses show that growth of the mixing layer is enhanced downstream of the origin, $0 < x < 80$; the growth rate of the mixing layer in this region is higher than the unforced mixing layers (Hereafter, this region is referred to as Region I). The plot of discrete vortices in figure 33(c) indicates that vortex amalgamation is enhanced in this region if compared with the unforced case. With further increasing downstream distance, say $80 < x < 160$, the growth of the mixing layer slows down or even stops (Region II). The plots of discrete vortices in this region show that lumps of discrete vortices or large eddies are aligned and no vortex pairing occurs in this region. Further downstream, $160 < x$, the mixing

layer recovers its growth with increasing x (Region III), as seen in figures 31 and 32. The behavior of discrete vortices in this region are quite similar to that in unforced mixing layers and the vortex pairing process was observed everywhere in this region. For a lower-frequency forced flow ($f = 0.08$), growth rate of a mixing layer is larger than that in the case of $f = 0.16$. The length of Region I when $f = 0.08$ is about twice the length than when $f = 0.16$, say $0 < x < 180$.

Velocity profiles of a low-frequency forced mixing layer ($f < f_p$) are shown in figures 34 and 35 for f=0.16. In the figures, the solid line indicates the similarity profile of the corresponding unforced mixing layer. We can see from figure 34 that the profiles of the mean velocity $\bar{u}$ are reasonably similar in all three regions owing to the choice of the similarity parameter η (Oster and Wygnanski, 1982). We can also see from figure 34 that the Reynolds stress is small everywhere in Region II and for sufficiently large forcing amplitudes it becomes negative across the mixing layer, indicating the occurrence of contra-gradient diffusion. The Reynolds stress is positive both in Region I and Region III. Figure 35 shows that the profiles of $r.m.s.\ u'$ are double-peaked in Region II where lumps of discrete vortices are aligned (figure 33(c)). The maximum value of the profile in the lower-speed region is approximately 0.15 which is in agreement with the value obtained by Oster and Wygnanski (1982). The profiles of $r.m.s.\ v'$ in figure 35 show that the peak values of $r.m.s.\ v'$ of forced mixing layers are larger than those of unforced mixing layers. The maximum value of $r.m.s.\ v'$ is about 0.3 and this value does not depend very much on the forcing amplitudes (see figure 36). Oster and Wygnanski (1982) determined the maximum value of $r.m.s.\ v'$ to be about 0.3 for the same velocity ratio, $r = 0.6$. The agreement between the calculation and the experiment is very good. It should be remembered that the difference of the $r.m.s.\ v'$ of unforced mixing layers between the calculation and the experiment is about twice (see table 2). Oster and Wygnanski (1982) showed that the flow becomes more two-dimensional when two-dimensional

forcing is applied. It is also interesting to note that in the experiment of a mixing layer with low Reynolds number, conducted by Browand and Weidman (1976), the results showed $r.m.s.\ u' < r.m.s.\ v'$ and also the deformed shape of $r.m.s.\ u'$. In low Reynolds number flows, small-scale streamwise vortices which are superimposed on large-scale spanwise vortices in high Reynolds number flows may be absent or at least weakened by the viscous effect, and thus low Reynolds number mixing layers could be more two-dimensional. Thus, the two-dimensional computational result $r.m.s.\ u' < r.m.s.\ v'$ and the deformed shape of $r.m.s.\ u'$, both of which are contradictory to experimental results when the Reynolds number is high, may be improved when the three-dimensional effects can be accounted for in the numerical simulations.

For a high frequency forced case ($f = 0.64$) which is about twice the predominant frequency f_p, the growth rates of all mixing layer thicknesses are much lower, in the region $x < 120$, than the growth rate of the unforced mixing layer: the growth of the mixing layer is suppressed (see figures 31 and 32). Suppression of a mixing layer for a high-frequency forcing was found numerically by Mansour (1985). The plot of discrete vortices in figure 33(e) shows that clusters of discrete vortices or large eddies are formed immediately downstream of the origin where no large eddies are formed for low frequency forced or unforced mixing layers . This flow feature is evident in figure 33(d) where the forced frequency, $f = 0.32$, is equal to the estimated predominant frequency, f_p. These large eddies do not show vortex pairing in the region where the growth rate of the mixing layer is suppressed. Further downstream, say $160 < x$, the forced mixing layer grows at nearly the same rate as that of the unforced mixing layer (see figures 31 and 32). In this region we can see vortex pairing process: the growth of a mixing layer is closely related to the vortex pairing.

Velocity profiles of a high-frequency forced mixing layer ($f > f_p$) are presented in figures 37 and 38 for f=0.64. The profiles of the mean velocity $\bar{u}$ in figure 37 are

similar because of the choice of the similarity parameter η, as in the case of a low-frequency forced mixing layer (figure 34). Figure 37 also shows that the Reynolds stress $-\overline{u'v'}$ is smaller than the values of unforced mixing layer in the region where the growth of the mixing layer is suppressed ($x < 120$), while it is larger in the region where the mixing layer grows at nearly the same growth rate as that of the unforced mixing layer. In comparison with the values of the unforced mixing layer, both $r.m.s.\ u'$ and $r.m.s.\ v'$ are small in the region where growth of the mixing layer is suppressed (see figure 38). With increasing downstream distance, both values of $r.m.s.\ u'$ and $r.m.s.\ v'$ increase and seem to attain the profile close to the similarity profile of the unforced mixing layer.

Effect of forcing frequency on the mean velocity profile is presented in figure 39. The velocity profile appears to be independent of the forcing frequency.

The effect of forcing amplitude on the development of a mixing layer is presented in figures 36 and 40-42 with $f = 0.16$. The difference of flows caused by the variation of forcing amplitude is shown in figure 43 with $t = 1000.0$. The effect of the forcing amplitude is not so drastic as is the effect of the forcing frequency (see figures 40 and 41). The profile of the mean velocity $\bar{u}$ in figure 36 shows that the profile appears to be independent of the forcing amplitude. Here it may be of interest to note that the profile of the mean velocity, $\bar{u}$, is approximately independent of both the velocity ratio r (figure 17) and the forcing frequency f (figure 39). Figure 42 shows that the defect of $r.m.s.\ u'$ and the negative value of the Reynolds stress in Region II become larger with increasing forcing amplitude.

Oster and Wygnanski (1982) systematically investigated the effect of initially forced periodic disturbances on the development of the turbulent mixing layers. Disturbances were imposed by an oscillating flap slightly downstream of the trailing edge of a splitter plate. The forced frequencies (from 20 to 100 Hz) were much smaller than the predominant frequency ($400Hz < f_p < 600Hz$) measured near

the trailing edge. They found that the development of the flow indicates different behavior in three regions. The first is the initial region in which the mixing layer grows with increasing x more rapidly than the unforced mixing layer. The second is the resonance region in which the growth of the layer slows down or even stops. The third is the downstream region in which the layer again grows at nearly the same rate as in the initial region. In the initial region the growth rate becomes larger with increase in amplitude of the forced disturbances, and the length of this region appeared to be inversely proportional to the frequency of the forced periodic disturbances. In the resonance region a single array of large, quasi-two-dimensional vortex lumps exists, which do not interact with one another. The double-peaked shape of $r.m.s.\ u'$ and the negative Reynolds stress are observed in the resonance region. The length of the resonance region is given by $1 \leq \lambda f x/U_c \leq 2$, where λ is defined as $\lambda = (U_1 - U_2)/(U_1 + U_2)$.

Most of the flow features of forced mixing layers observed experimentally by Oster and Wygnanski (1982) are reproduced here for the cases of low-frequency forcing ($f < f_p$). The three regions observed by Oster and Wygnanski (1982) correspond to the Regions I through III in this calculation. The criterion for the length of the resonance region is also satisfied. For example, the resonance region is $80 \leq x \leq 160$ for $f = 0.16$, as seen in figures 31 and 32, and $\lambda = 0.25, U_c = 3.2$ in this calculation.

Zaman and Hussain (1980) imposed disturbances on the origin of a mixing layer using sound from a loudspeaker. Their results showed that turbulence suppression, or reduction of turbulent intensity, occurs when the forcing frequency f is larger than the predominant frequency f_p. Zaman and Hussain (1980) speculate that turbulent suppression is a consequence of earlier transition, induced by the forcing, of the shear layer vortices which otherwise naturally grow to larger sizes and undergo successive pairing in the corresponding unforced flow. Our results shown in figures 33(d), (e) and figure 38 indicate that turbulent suppression is related to inhibition of vortex

pairing and thus are consistent with the observation of Zaman and Hussain (1980).

Recently, Bell and Mehta (1985) investigated the effect of initial, periodic disturbances on a 2D mixing layer. Disturbances are provided at the trailing edge of the splitter plate using an oscillating flap. Their results showed, consistent with our calculated results, that vortex pairing is enhanced shortly downstream of the splitter plate for low-frequency forced cases while suppressed for high-frequency forced cases.

Finally, both the effects of forcing amplitude and forcing frequency on the normal velocity V on the walls are shown in figure 44. Clearly, both forcing amplitude and forcing frequency have little influence on the normal velocity.

SUMMARY AND CONCLUDING REMARKS

Spatially growing, turbulent mixing layers with and without forcing were simulated numerically by a 2D vortex method. Many of the flow features which have been observed experimentally are reproduced, and good quantitative agreement between experiments and computations is obtained. The main conclusions of this study are as follows. First, the time-averaged flow quantities up to third-order moments show similarity for unforced mixing layers. The peak values of both *r.m.s.* u' and $-\overline{u'v'}$ are in agreement with experimental values, while the peak values of *r.m.s.* v' are approximately twice as high as the experimental ones. The peak values of third-order quantities are approximately two times the value of those found experimentally. Second, the peak value of *r.m.s.* u' is smaller than *r.m.s.* v' in every case of unforced mixing layers treated in this paper. This result is contradictory to experimental results obtained when the Reynolds number is high. The result for forced mixing layers suggests that three dimensionality existing in actual flows may be responsible. Third, the profiles of both $\overline{u'^3}$ and $\overline{u'v'^2}$ show bumps near the boundaries of a mixing layer, which have not been observed in experiments. Along with the deformed shape of *r.m.s.* u' which has been observed in a low Reynolds number mixing layer,

these problems may also be associated with the three dimensionality of the flow, though further confirmation is needed. Fourth, the calculated results are consistent with experiments for forced mixing layers.

This study suggests that vortex methods may be quite effective and useful to simulate turbulent mixing layers, and that studying the effect of three dimensionality on flow feature : will be an important continuation of this work.

ACKNOWLEDGMENTS

We express our thanks to Drs. N. N. Mansour, P. R. Spalart, R. D. Mehta, and K. Shariff, at NASA Ames Research Center, for valuable advice and fruitful discussions. Thanks are also given to Mr. W. M. Younkin, Control Data Corporation, for his kind advice on the use of the Cyber 205.

REFERENCES

Aref, H.: Integrable Chaotic, and Turbulent Vortex Motion in Two Dimensional Flows. Ann. Rev. Fluid Mech., vol.15, 1983, pp. 345-389.

Ashurst,W.T.: Numerical Simulation of Turbulent Mixing Layers via Vortex Dynamics. Turbulent Shear Flows. vol.I, edited by Durst et al., Springer-Verlag, New York, 1979, pp. 402-413.

Bell, J.H.; and Mehta, R.D.: Perturbed Mixing Layers. Bull. American Phys. Soc., vol.30, No.10, 1985, p. 1744.

Browand, F.K.; and Weidman, P.D.: Large Scales in the Developing Mixing Layer. J. Fluid Mech., vol.76, 1976, pp. 127-144.

Ho, C.M.; and Huang, L.S.: Subharmonics and Vortex Merging in Mixing Layer. J. Fluid Mech., vol.119, 1982, pp. 443-473.

Ho,C.M.; and Huerre, P.: Perturbed Free Shear Layers. Ann. Rev. Fluid Mech., vol.16, 1984, pp. 365-424.

Inoue, O.: Simulation of Initially Forced Mixing Layers. J. Phys. Soc. Japan, vol.54, January, 1985a, pp. 121-133.

Inoue, O.: Vortex Simulation of a Turbulent Mixing Layer. AIAA J., vol.23, March, 1985b, pp. 367-373.

Leonard, A.: Computing Three-Dimensional Incompressible Flows with Vortex Elements. Ann. Rev. Fluid Mech., vol.17, 1985, pp. 523-559.

Mansour, N.N.: Simulation of Turbulent Mixing Layers. Fifth Symposium on Turbulent Shear Flows. Ithaca, NY, 1985, pp. 3.33-3.38. (See also Sandia Report SAND 84-8940, Sandia National Laboratories, California 94550).

McInville, R.M.; Gatski, T.B.; and Hassan, H.A.: Analysis of Large Vortical Structures in Shear Layers. AIAA J., vol.23, 1985, pp. 1165-1171.

Mehta, R.D.; and Westphal, R.V.: An Experimental Study of Plane Mixing Layer Development. NASA TM 86698, 1985.

Michalke, A.: Vortex Formation in a Free Boundary Layer According to Stability Theory. J. Fluid Mech., vol.22, 1965, pp. 371-383.

Oster,D.; and Wygnanski,I.: The Forced Mixing Layer between Parallel Streams. J. Fluid Mech., vol.123, 1982, pp. 91-130.

Saffman, P.G.; and Baker, G.R.: Vortex Interactions. Ann. Rev. Fluid Mech., vol.11, 1979, pp. 95-122.

Spencer,B.W., Ph.D Thesis, Nuclear Engineering Program, University of Illinois, Urbana, 1970. (From Ref.10).

Spencer,B.W.; and Jones,B.G.: Statistical Investigation of Pressure and Velocity Fields in the Turbulent Two-Stream Mixing Layer. AIAA Paper 71-613, June, 1971.

Yule, A.J.: Aeronautical Research Council, London, R & M 3683, 1971. (From Ref.10).

Zaman,K.B.Q.M.; and Hussain,A.K.M.F.: Vortex Pairing in a Circular Jet under Controlled Excitation: Part I. General Jet Response, J. Fluid Mech., vol.101, 1980, pp. 449-491.

Table.1. Effect of parameters on mean flow quantities at r=0.6 and U_c=3.2.

Case No.		Parameters				Results			
		x_{max}	L	ε	N_{up}	db/dx	u'/ΔU	v'/ΔU	$\overline{-u'v'}/\Delta U^2$
Case 1.	Long Calculation	500	± 50	0.6ℓ	1000	0.049	0.198	0.254	0.012
Case 2.	Standard case	500	± 50	0.6ℓ	1000	0.049	0.194	0.250	0.012
Case 3.	Effect of core (ε)	500	± 50	0.3ℓ	1000	0.048	0.204	0.257	0.014
Case 4.	Effect of core (ε)	500	± 50	0.15ℓ	1000	0.046	0.204	0.262	0.012
Case 5.	Effect of wall (L)	500	± 70	0.6ℓ	1000	0.049	0.198	0.250	0.012
Case 6.	Effect of wall (L)	500	± 30	0.6ℓ	1000	0.047	0.192	0.250	0.012
Case 7.	Effect of wall (L)	500	± 10	0.6ℓ	1000	0.043	0.182	0.250	not similar
Case 8.	Without wall	500	-	0.6ℓ	1000	0.046	0.192	0.250	0.014
Case 9.	Effect of N_{up}	500	± 50	0.6ℓ	500	0.052	0.200	0.245	0.015
Case 10.	Effect of x_{max}	350	± 50	0.6ℓ	1000	0.047	0.200	0.250	0.013
Case 11.	Model B (1)	500	± 50	0.6ℓ	1000	0.049	0.196	0.256	0.013
Case 12	Model B (2)	500	± 30	0.6ℓ	1000	0.049	0.198	0.250	0.013
Case 13.	Model C (1)	500	± 50	0.6ℓ	1000	0.047	0.202	0.250	0.013
Case 14.	Model C (2)	500	± 30	0.6ℓ	1000	0.051	0.199	0.250	0.013

Table.2. Comparison of this study with experiments for Model A with $L = 50.0$.

LIST OF FIGURES

Velocity ratio	Source	db/dx	dθ/dx	$d\theta_e/dx$	$dy_{0.5}/dx$	u'/ΔU	v'/ΔU	$-\overline{u'v'}/\Delta U^2$
r = 0.6	**Oster & Wygnanski** (1982)	0.045	0.009		- 0.004	0.180	0.153	0.013
	Yule (1971)	0.054				0.173	0.16	0.013
	Spencer (1970)					0.17	0.14	0.011
	Spencer & Jones (1971)				- 0.005	0.19	0.12	
	This study (200≤t≤1,400)	0.049	0.010	0.015	- 0.006	0.194	0.25	0.012
	This study (200≤t≤11,000)	0.049	0.010	0.015	- 0.006	0.198	0.254	0.012
r = 0.46	**Mehta & Westphal** (1985) **(1) TST**	0.054	0.012			0.179	0.118	0.011
	Mehta & Westphal (1985) **(2) TSU**	0.063	0.013			0.187	0.126	0.012
	This study	0.061	0.013	0.021	- 0.012	0.198	0.25	0.012
r = 0.3	**Oster & Wygnanski** (1982)	0.100	0.019		- 0.026	0.179		
	Spencer & Jones (1971)				- 0.020	0.19	0.13	0.013
	This study	0.105	0.020	0.031	- 0.024	0.191	0.25	0.012

** $b = y_{0.95} - y_{0.1}$ for r = 0.6 and 0.3, while $b = y_{0.9} - y_{0.1}$ for r = 0.46.

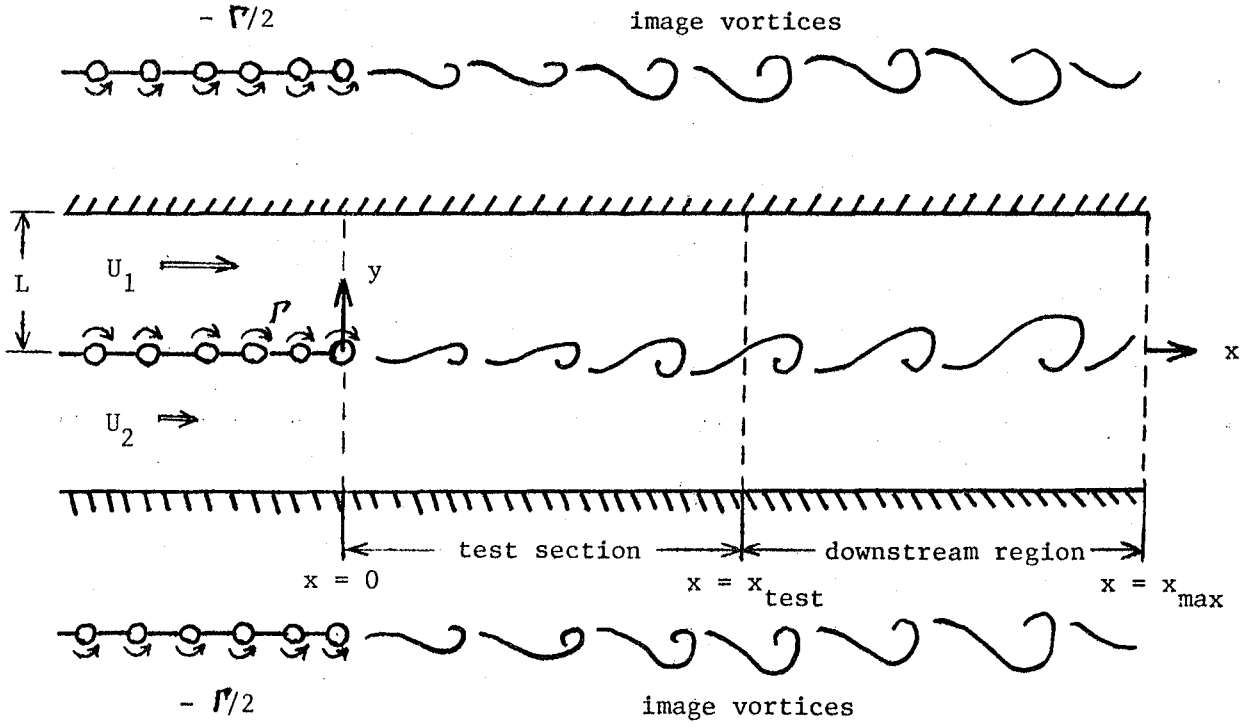

Fig.1. Schematic of flow for Model A.

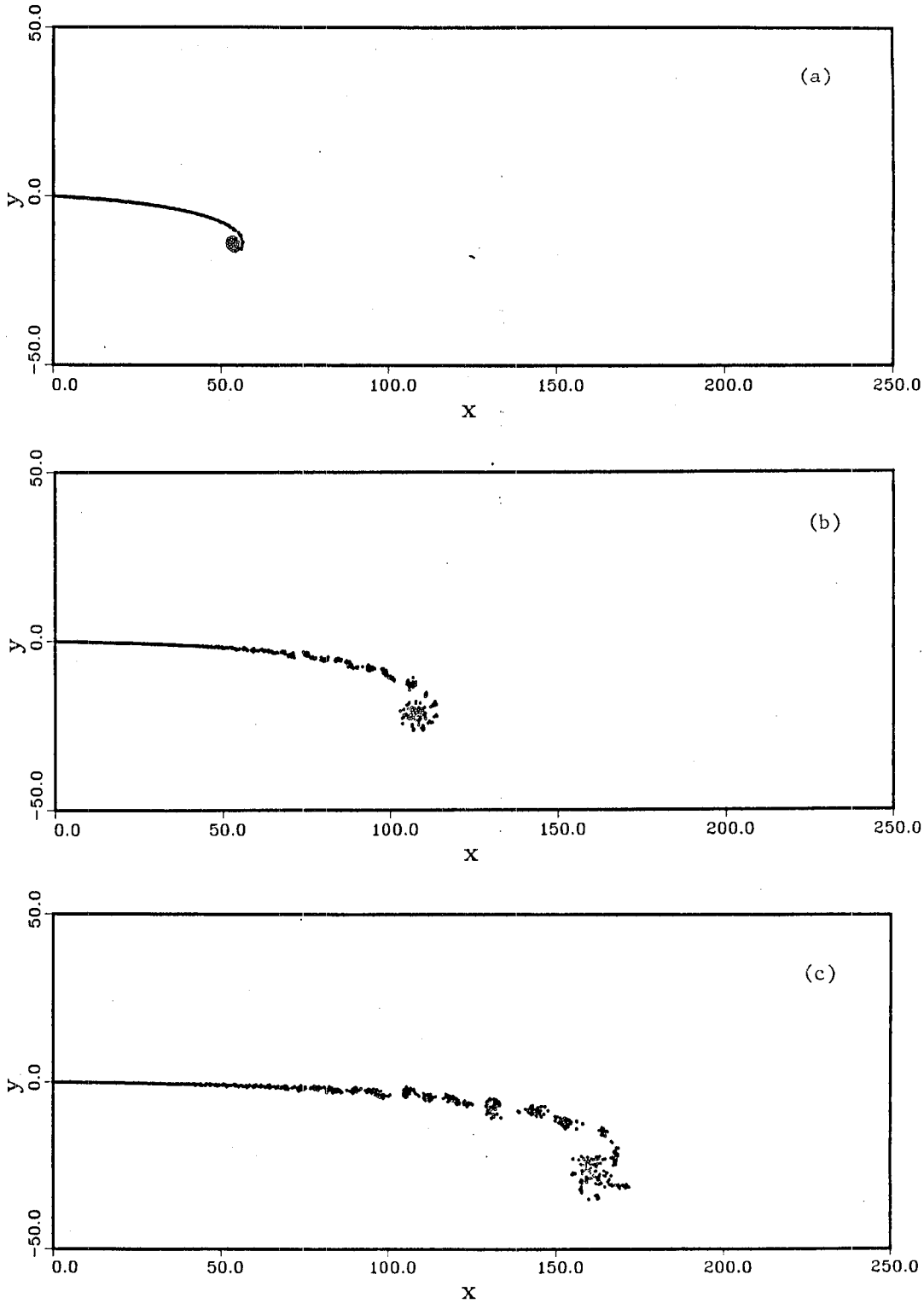

Fig.2. Flow at the initial stage of time development at $r = 0.6$. (a) $t = 20.0$, (b) $t = 40.0$, (c) $t = 60.0$

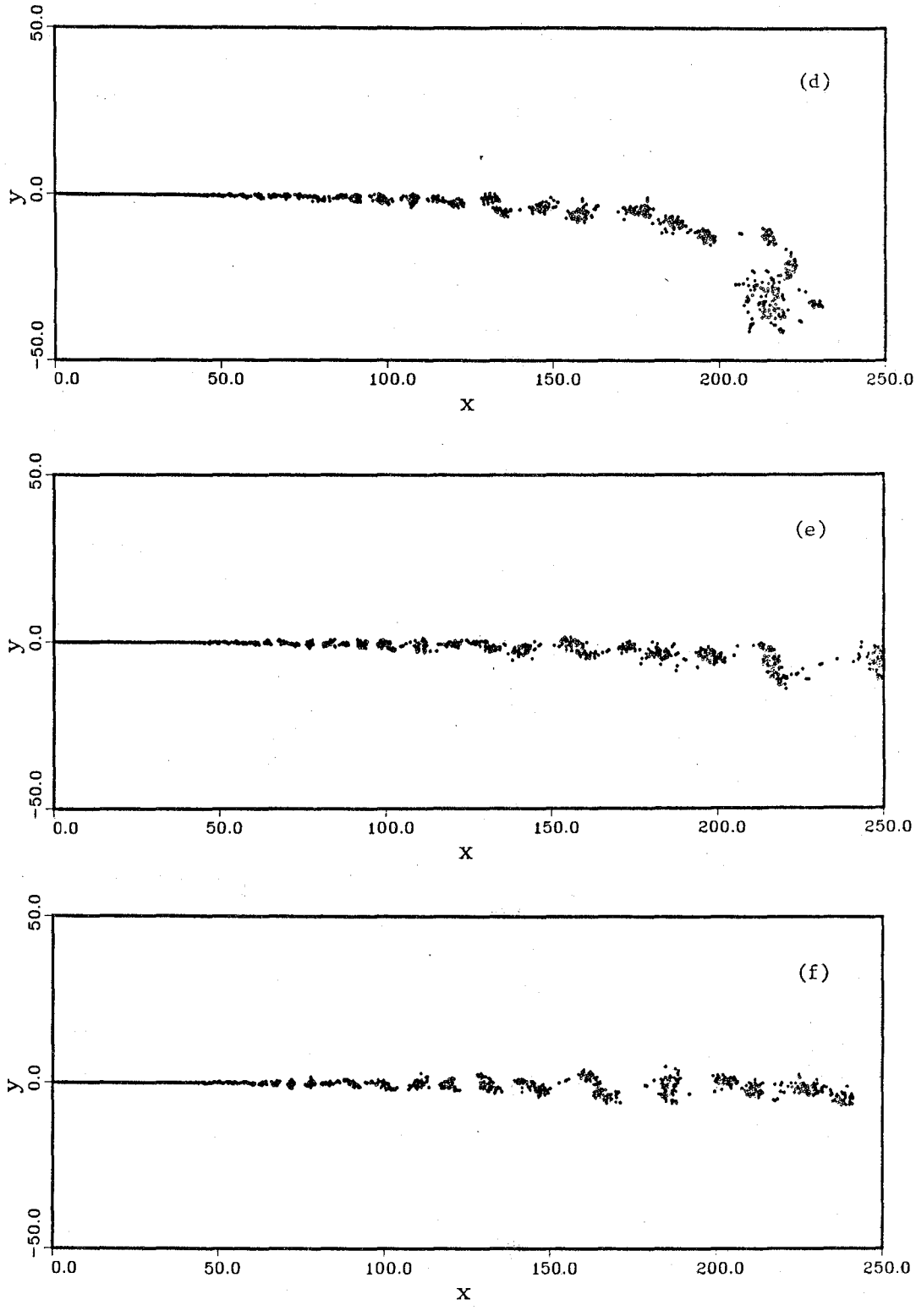

Fig.2. - continued. (d) $t = 80.0$, (e) $t = 100.0$, (f) $t = 140.0$

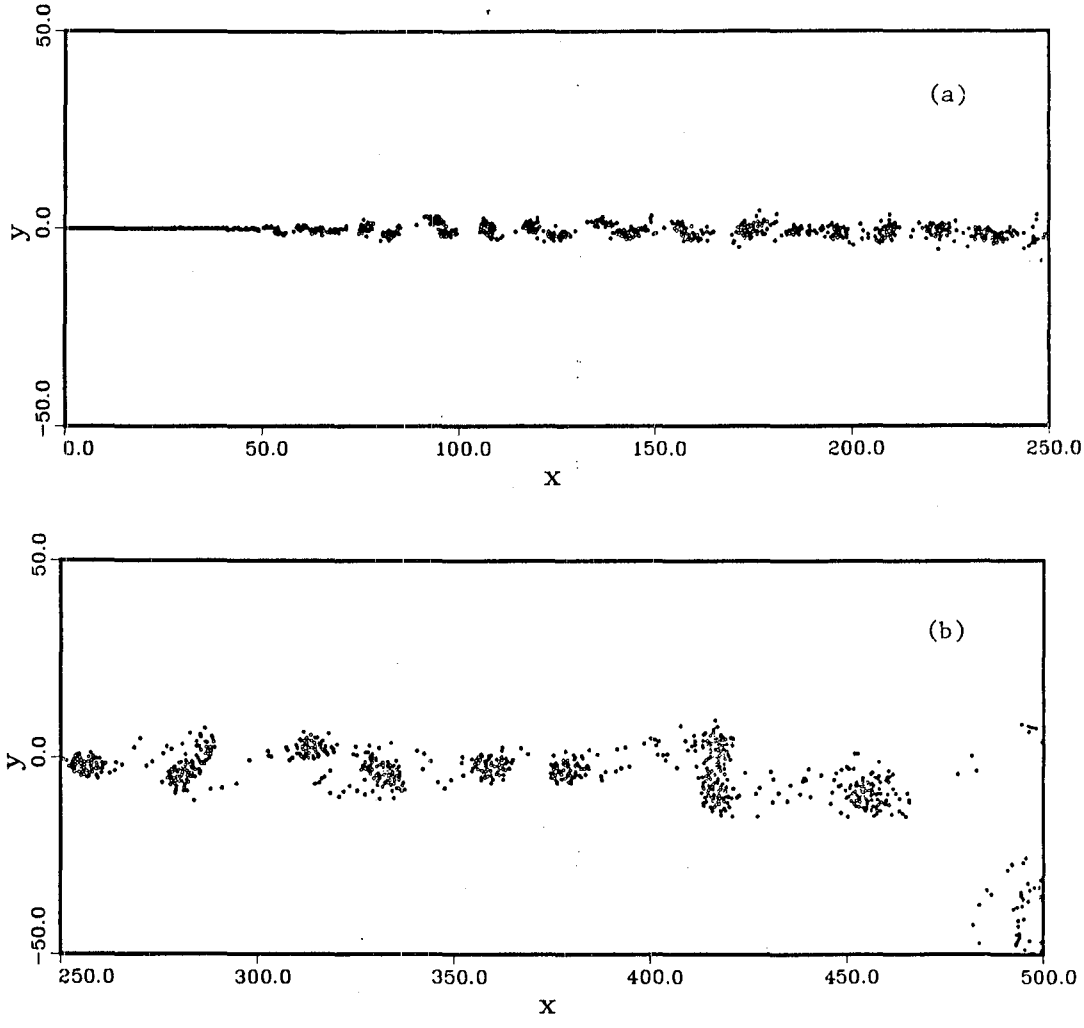

Fig.3. Flow at the start of velocity measurement at $t = 200.0$ and $r = 0.6$. (a) The test section, $0.0 \leq x \leq 250.0$ (b) the downstream region, $250.0 \leq x \leq 500.0$

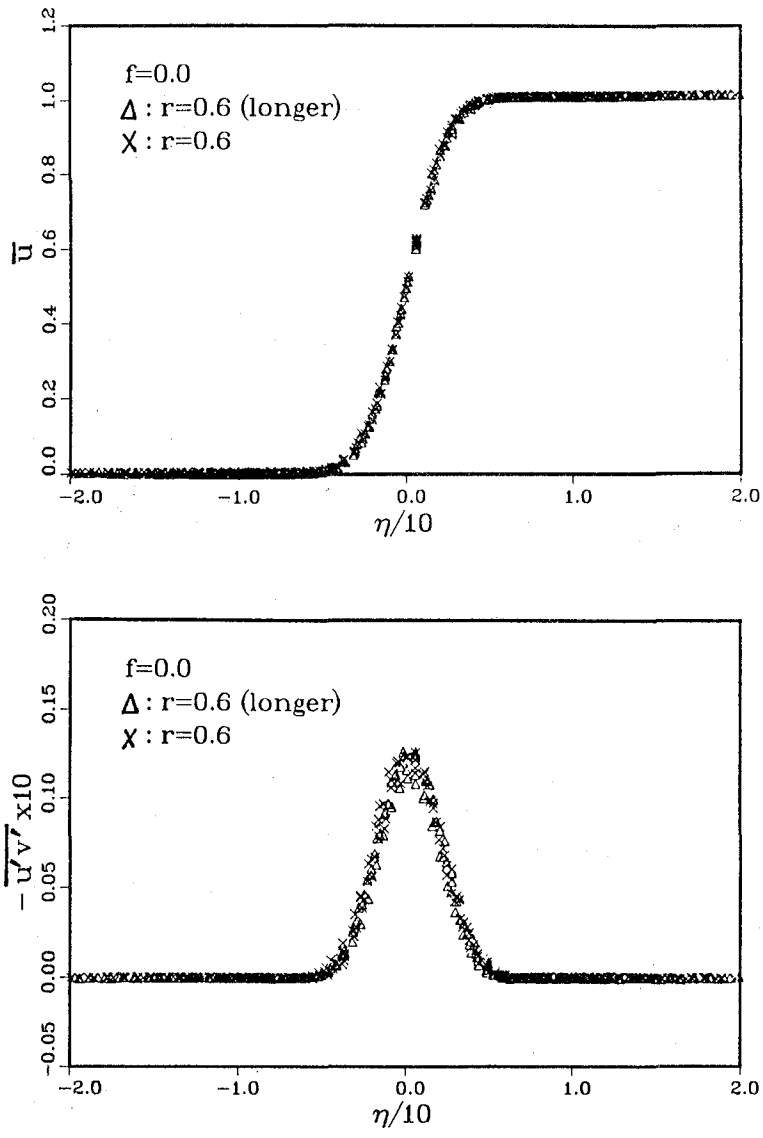

Fig.4 . Effect of the difference in averaging time on $\bar{u}$ and $-\overline{u'v'}$ at x=120, 140 160, 180, and 200.

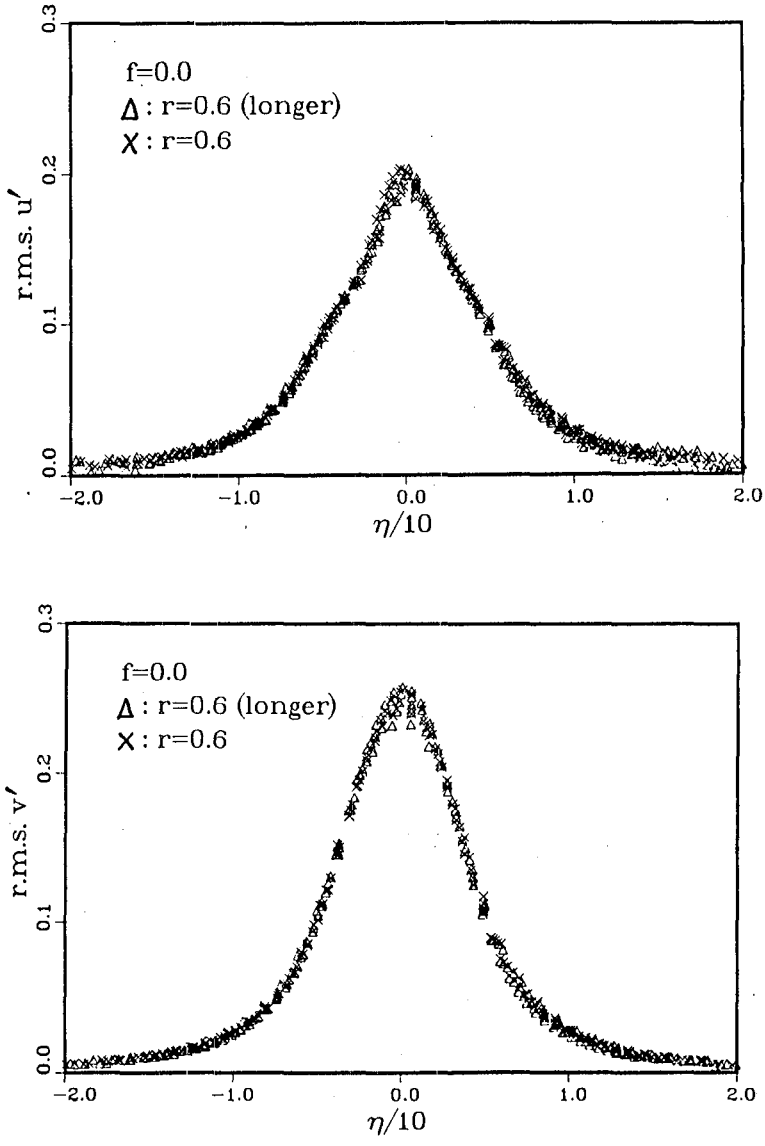

Fig.5 . Effect of the difference in averaging time on *r.m.s.* u' and *r.m.s.* v' at x=120, 140, 160, 180, and 200.

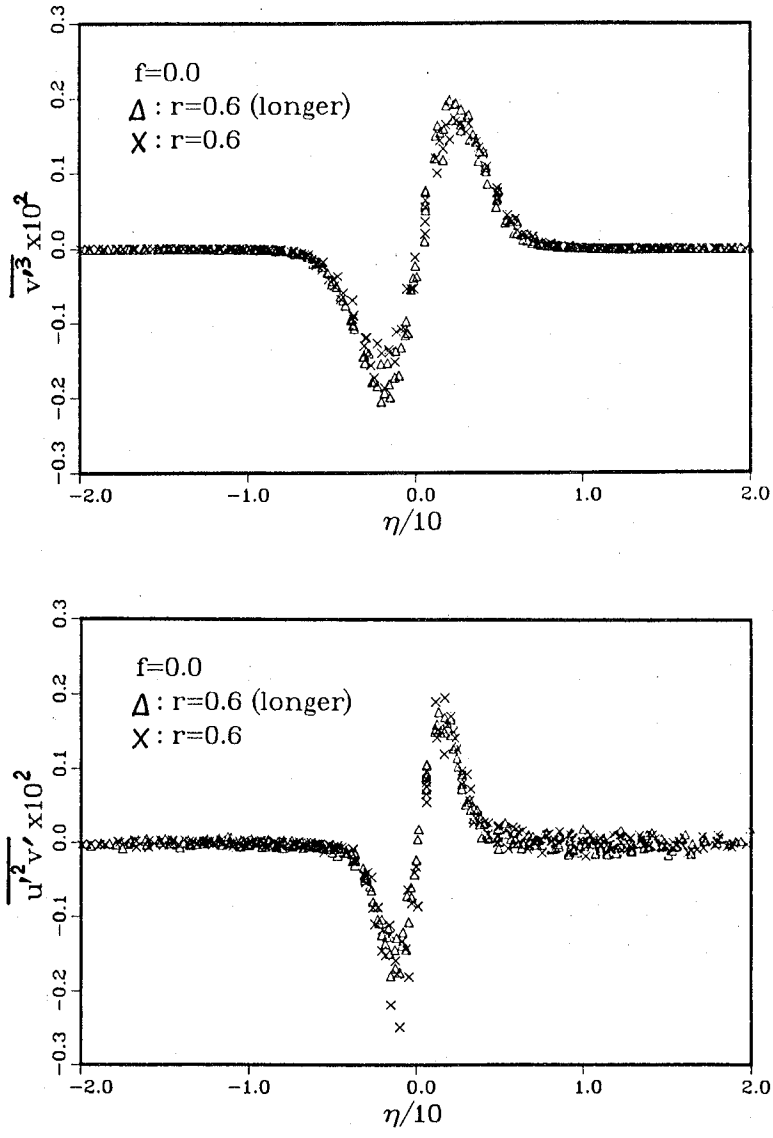

Fig.6 . Effect of the difference in averaging time on $\overline{vl^3}$ and $\overline{ul^2v'}$ at x=120, 140, 160, 180, and 200.

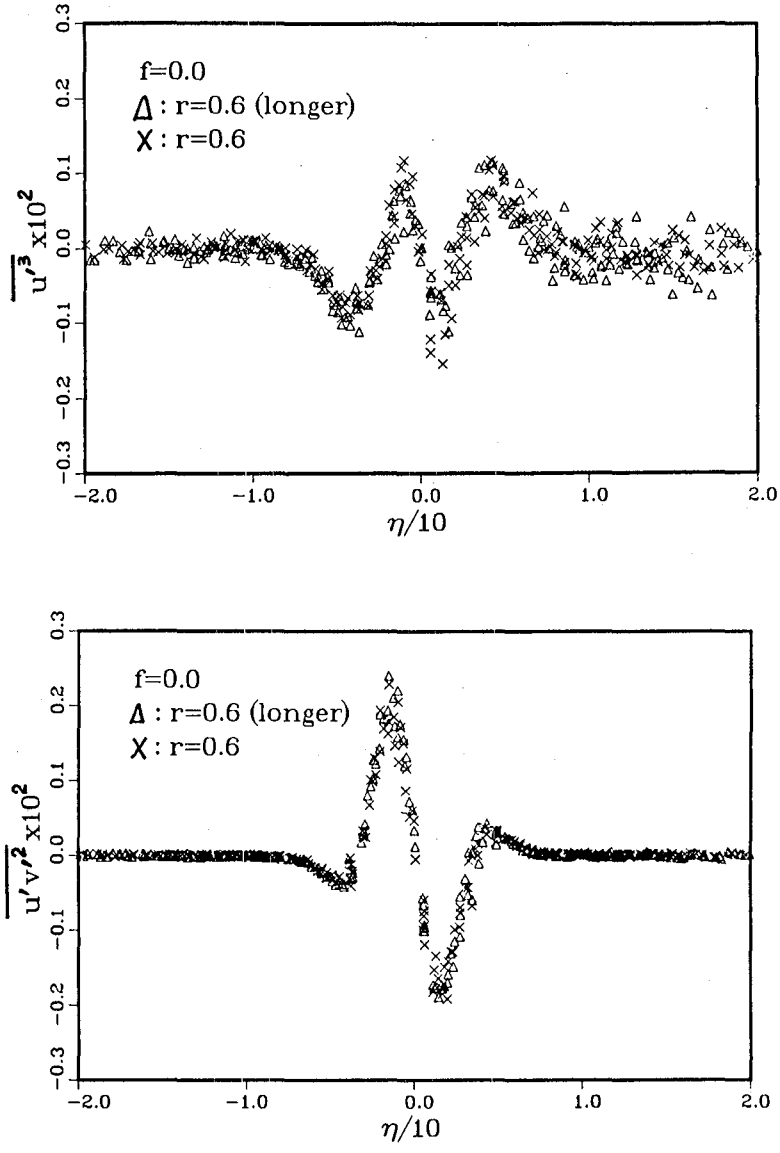

Fig.7 . Effect of the difference in averaging time on $\overline{ul^3}$ and $\overline{u'vl^2}$ at x=120, 140, 160, 180, and 200.

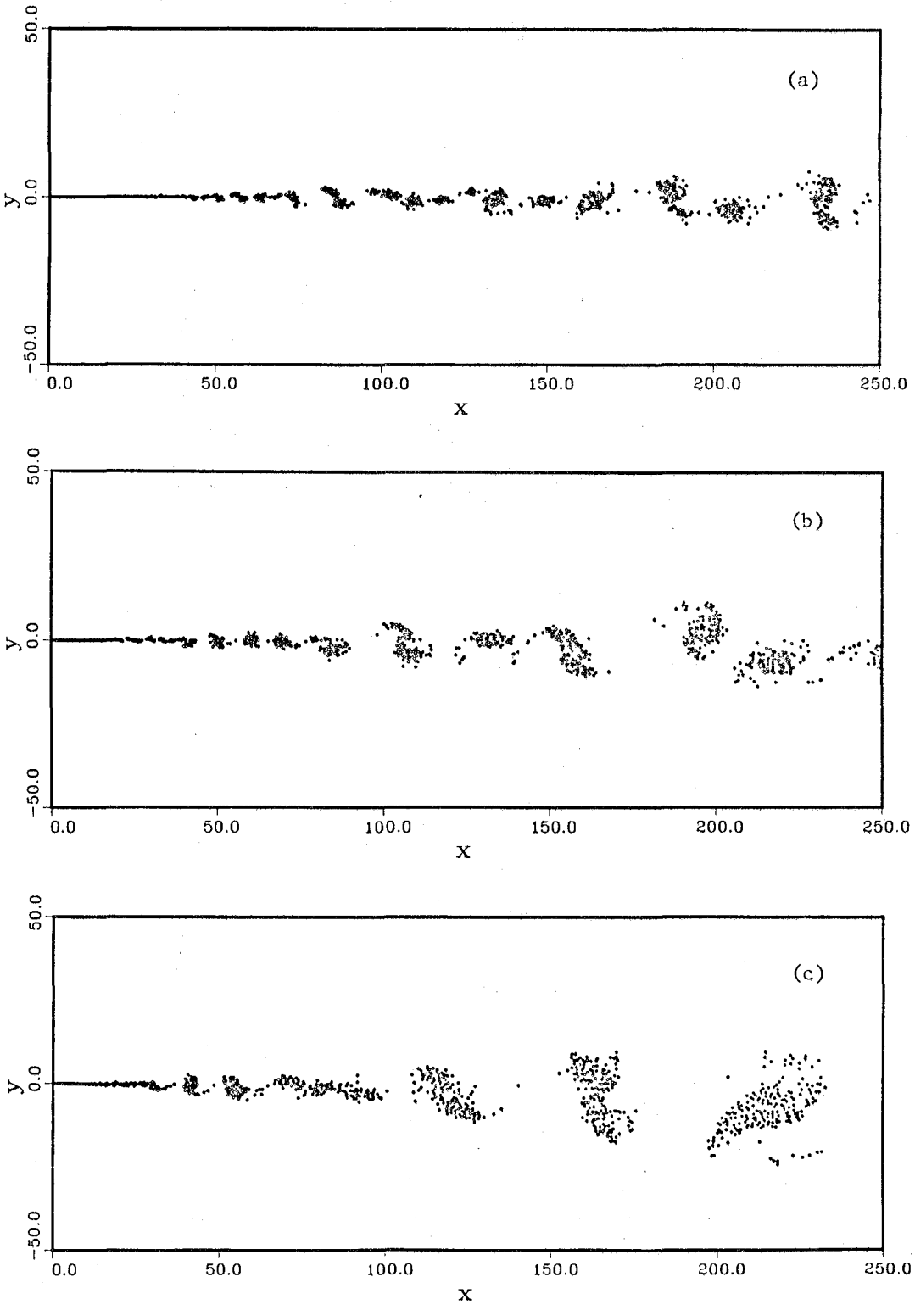

Fig.8. Flow in a quasi-steady state at $t = 1000.0$. a) $r = 0.6$ b) $r = 0.46$ c)$r = 0.3$

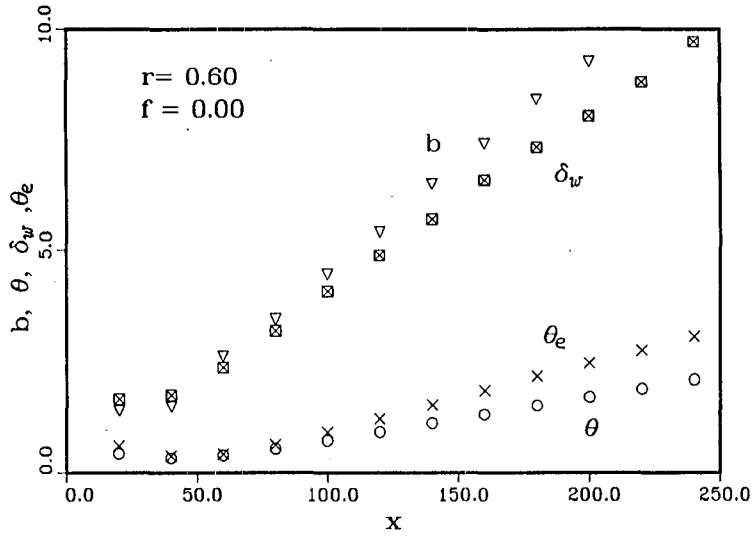

Fig.9. Growth of a mixing layer at $r = 0.6$ (1). ○: θ, ▽: b, ⊠: δ_w, X: θ_e.

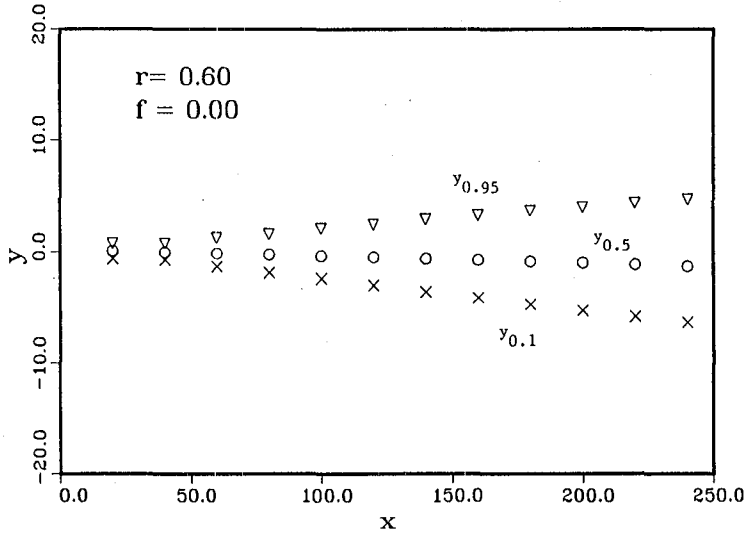

Fig.10. Growth of a mixing layer at $r = 0.6$ (2). ▽: $y_{0.95}$, ○: $y_{0.5}$, X: $y_{0.1}$.

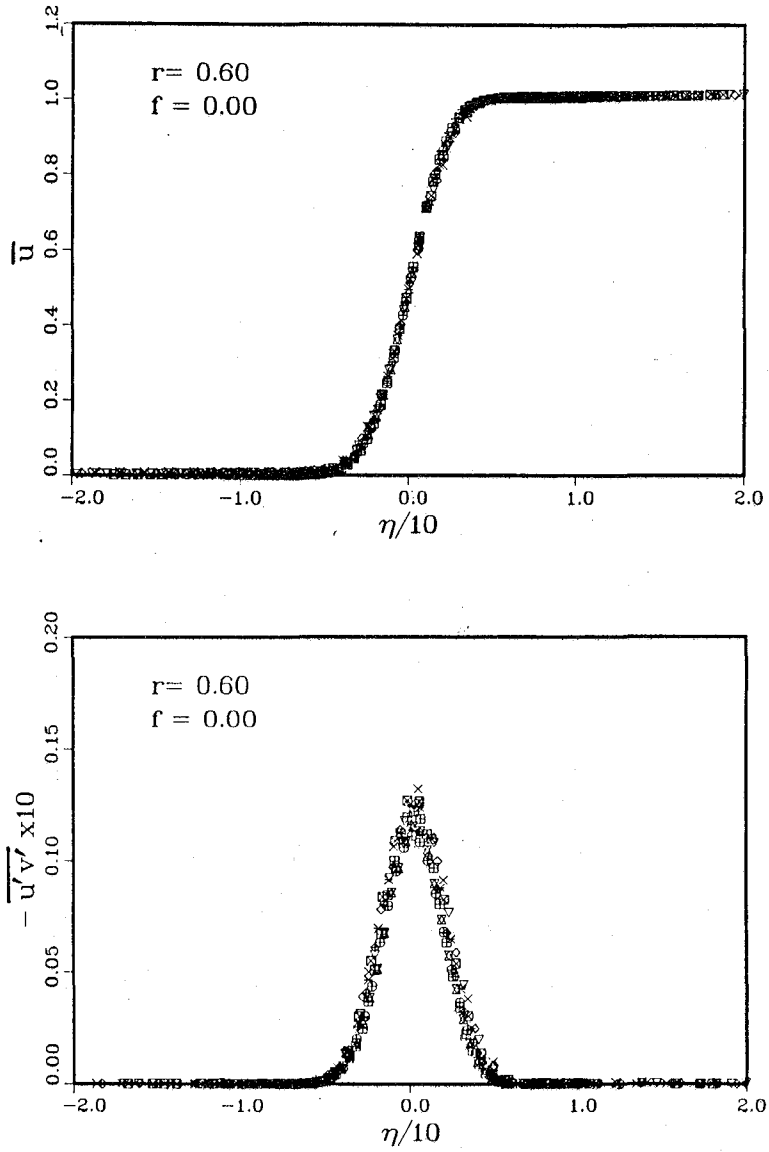

Fig.11. Mean Velocity $\bar{u}$ and the Reynolds stress $-\overline{u'v'}$. $r = 0.6$. $\times: x = 80$, $\diamond: x = 100$, $\nabla: x = 120$, $\boxtimes: x = 140$, $*: x = 160$, $\diamond: x = 180$, $\oplus: x = 200$, $\boxtimes: x = 220$, $\boxplus: x = 240$.

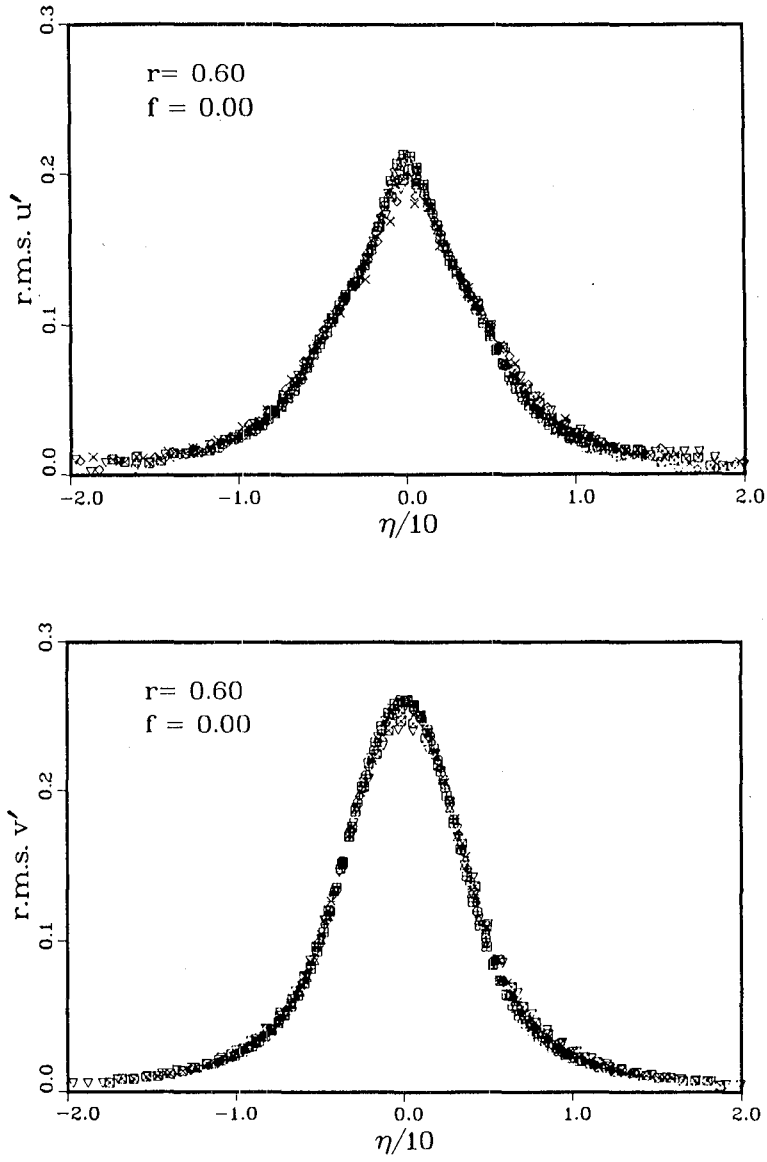

Fig.12. Fluctuation velocities *r.m.s.* u' and *r.m.s.* v'. $r = 0.6$. (For legend, see Fig.11)

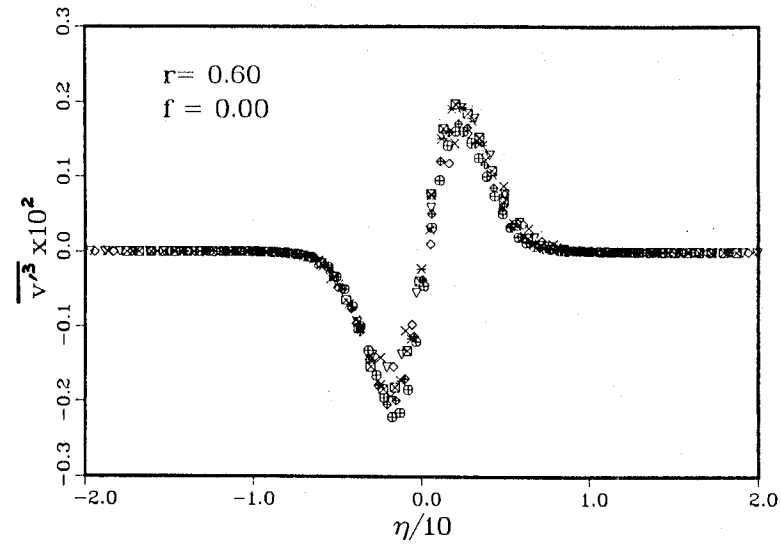

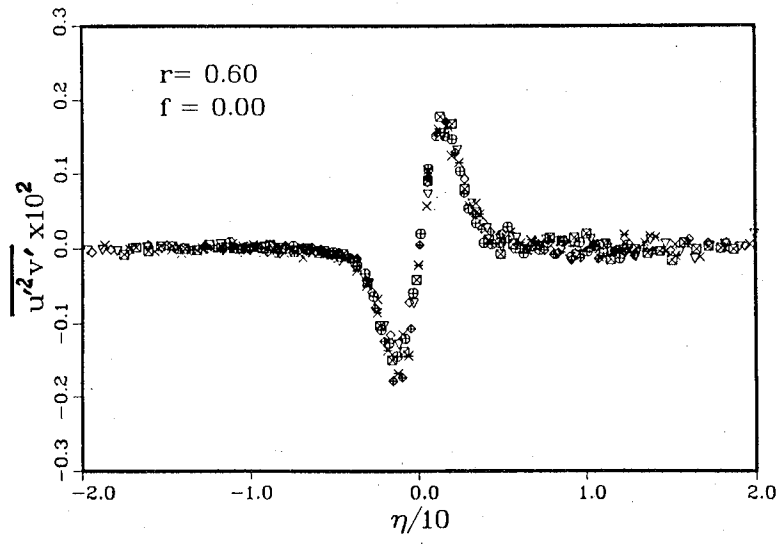

Fig.13. Third-order moments (1). $\overline{v'^3}$ and $\overline{u'^2v'}$. $r = 0.6$. (For legend, see Fig.11)

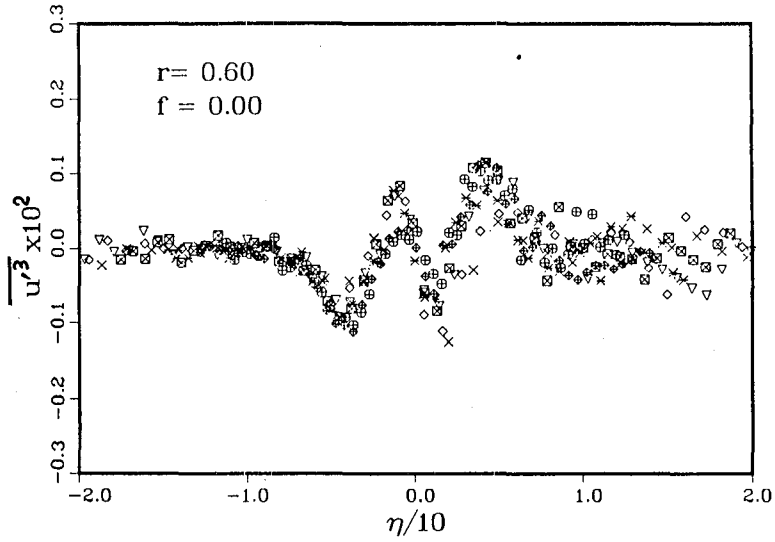

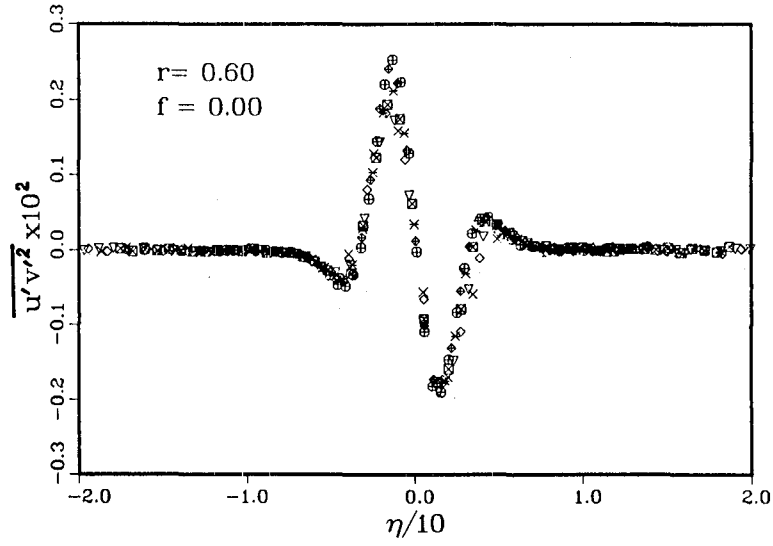

Fig.14. Third-order moments (2). $\overline{ul^3}$ and $\overline{u'vl^2}$. $r = 0.6$. (For legend, see Fig.11.)

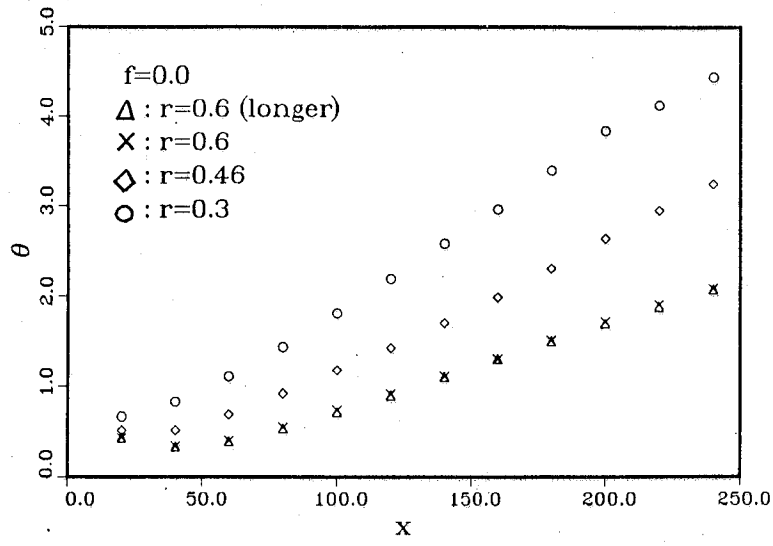

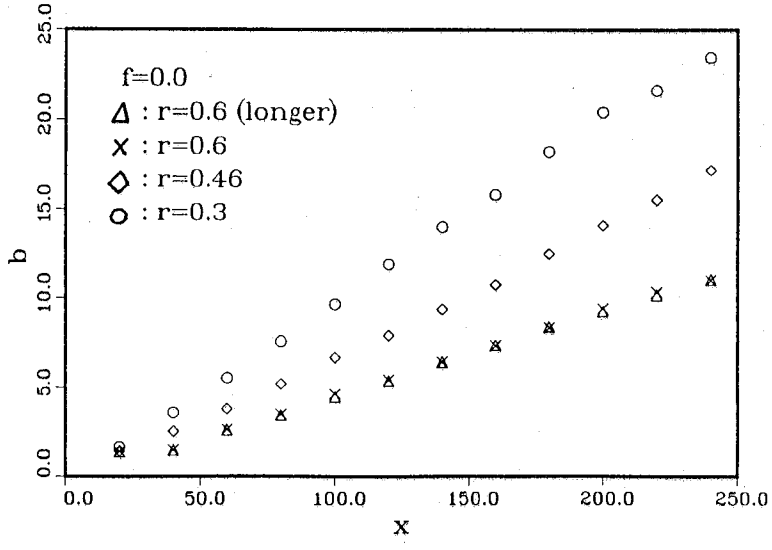

Fig.15. Effect of r on the growth of a mixing layer for momentum thickness θ and mixing layer thickness b.

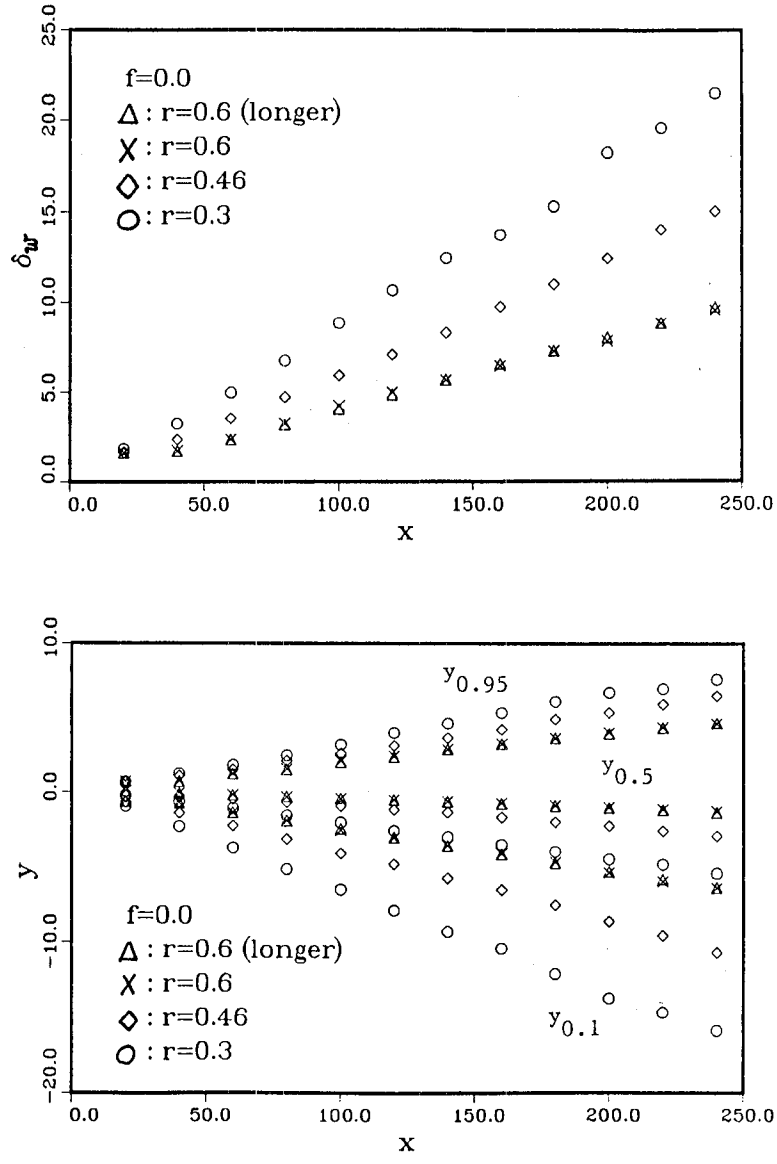

Fig.16. Effect of r on the growth of a mixing layer for vorticity thickness δ_w and the positions of $y_{0.95}$, $y_{0.5}$ and $y_{0.1}$.

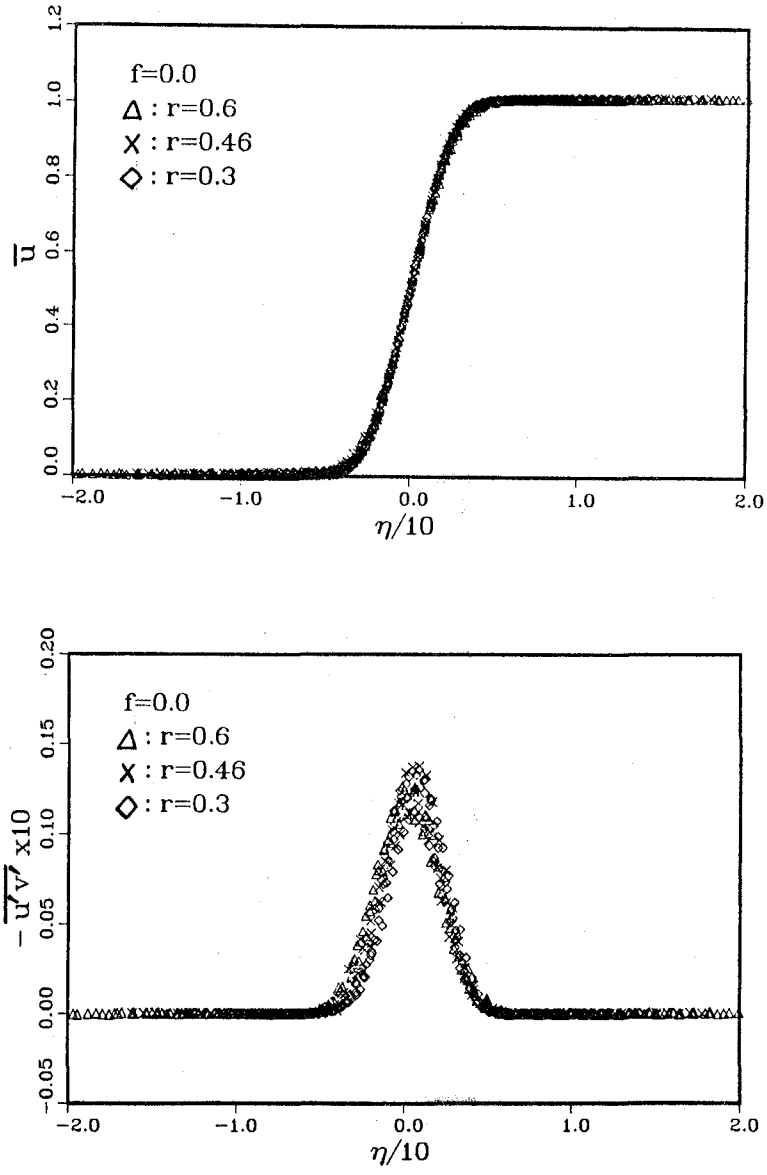

Fig.17. Effect of r on the mean velocity $\bar{u}$ and the Reynolds stress $-\overline{u'v'}$ at x=120, 140, 160, 180, and 200.

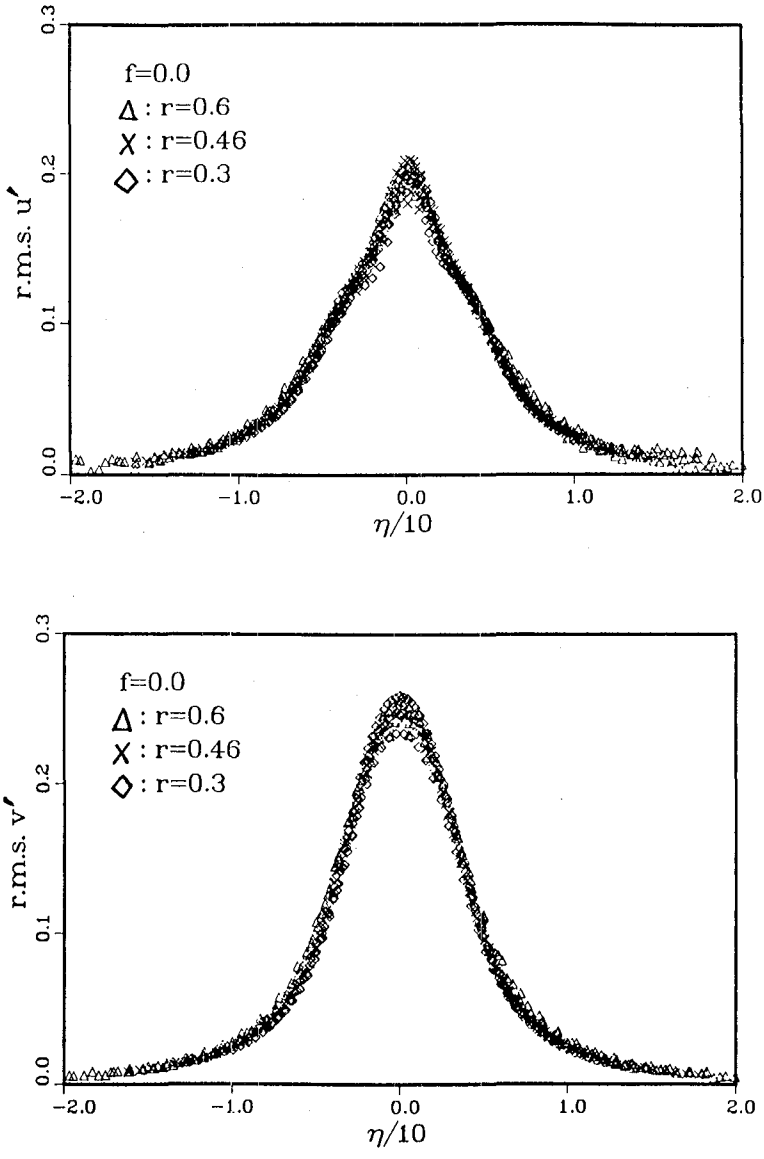

Fig.18. Effect of r on $r.m.s.\ u'$ and $r.m.s.\ v'$ at x=120, 140, 160, 180, and 200.

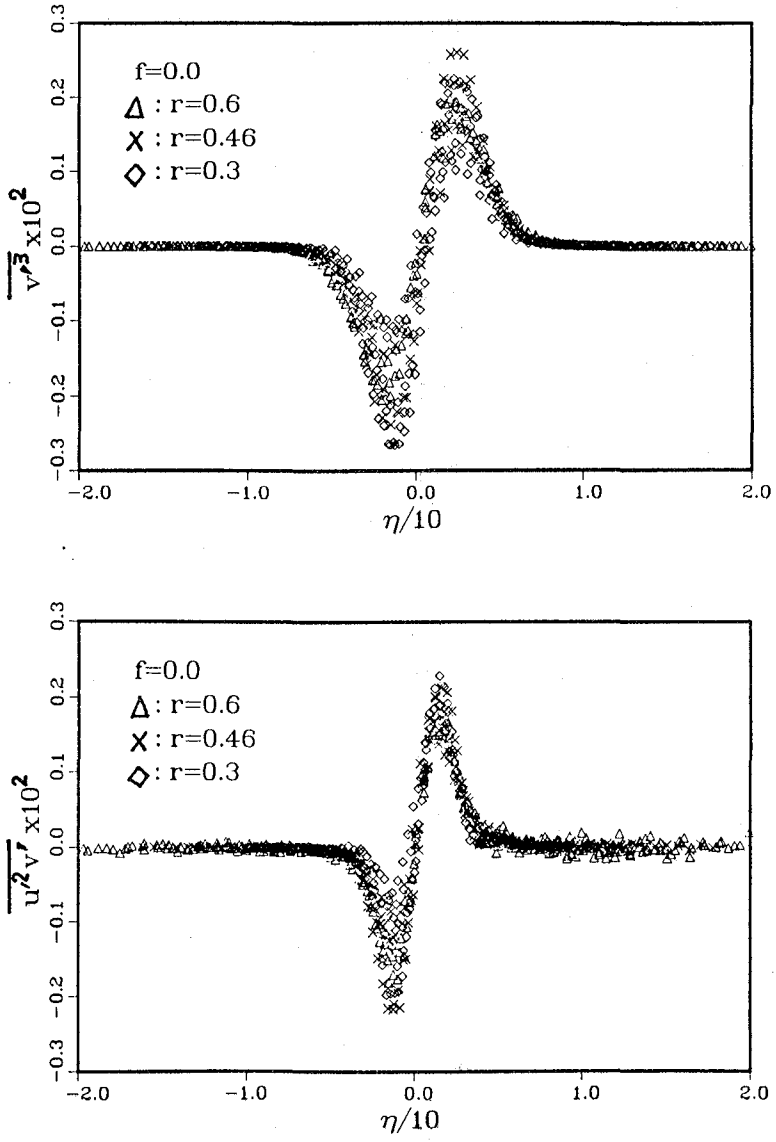

Fig.19. Effect of r on $\overline{vl^3}$ and $\overline{ul^2v'}$ at x=120, 140, 160, 180, and 200.

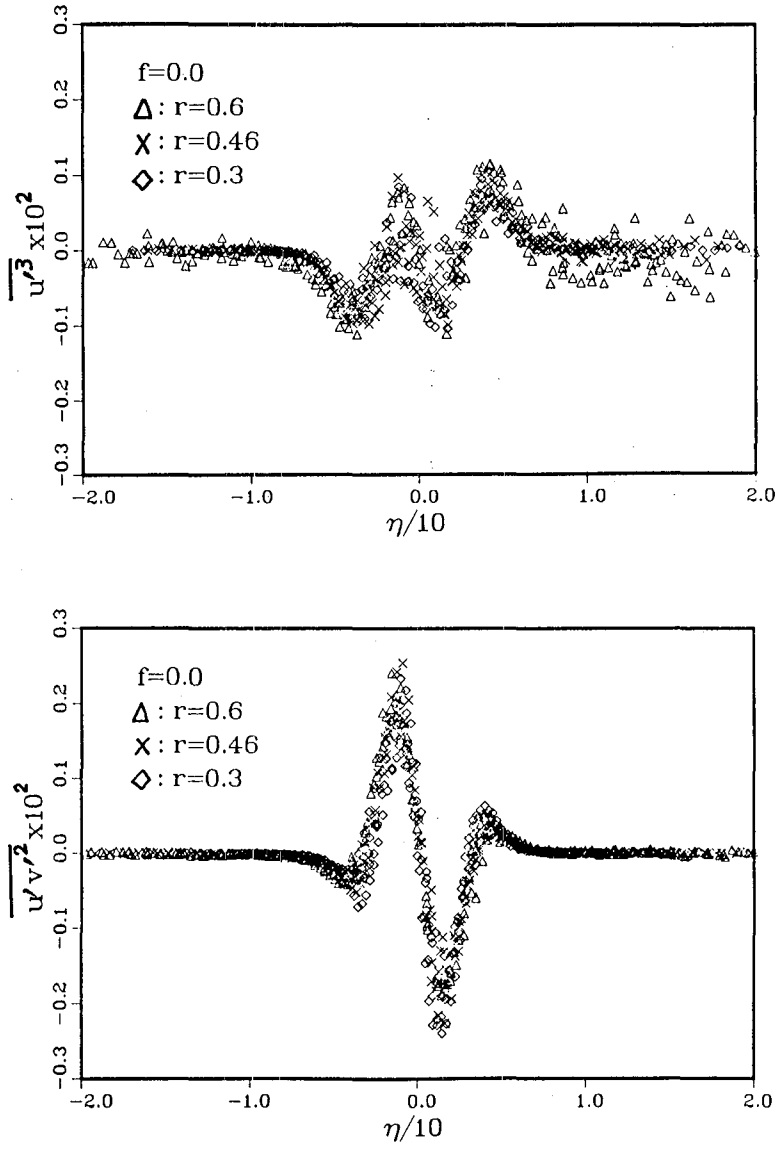

Fig.20. Effect of r on $\overline{ul^3}$ and $\overline{u'vl^2}$ at x=120, 140, 160, 180, and 200.

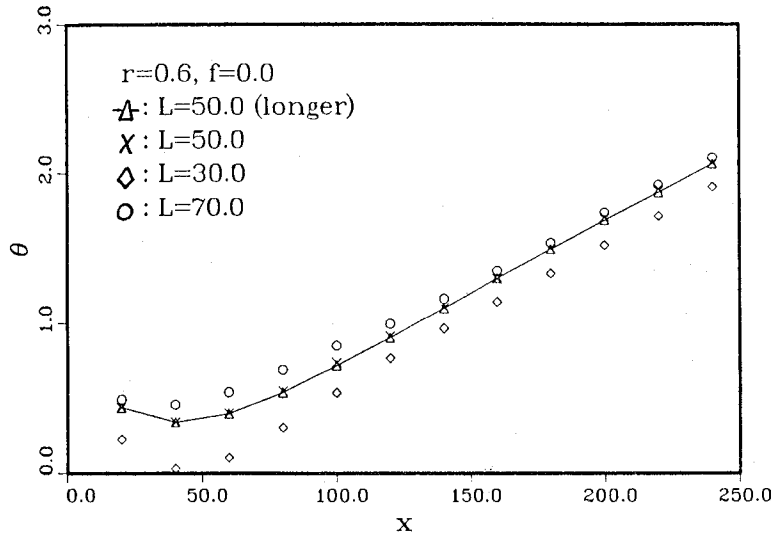

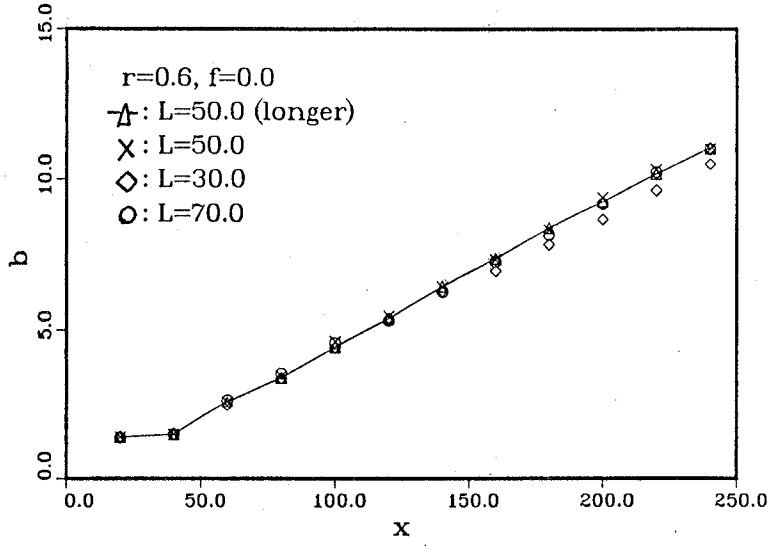

Fig.21. Effect of L on the growth of a mixing layer for momentum thickness θ and mixing layer thickness b.

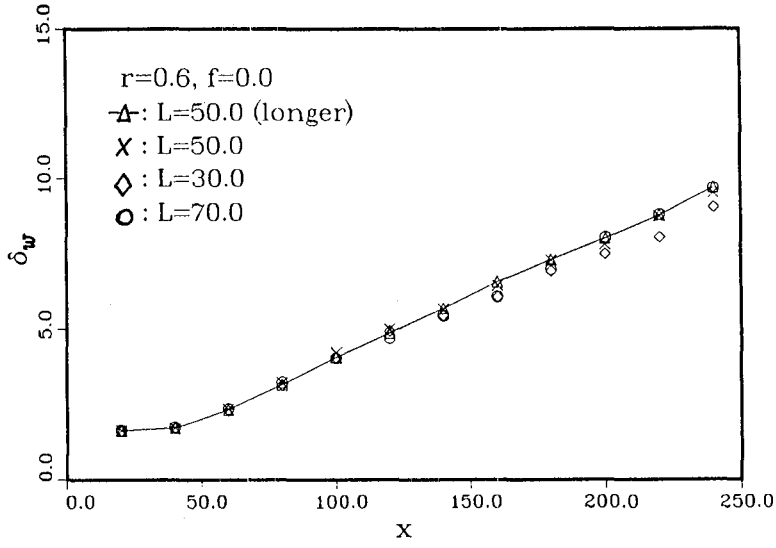

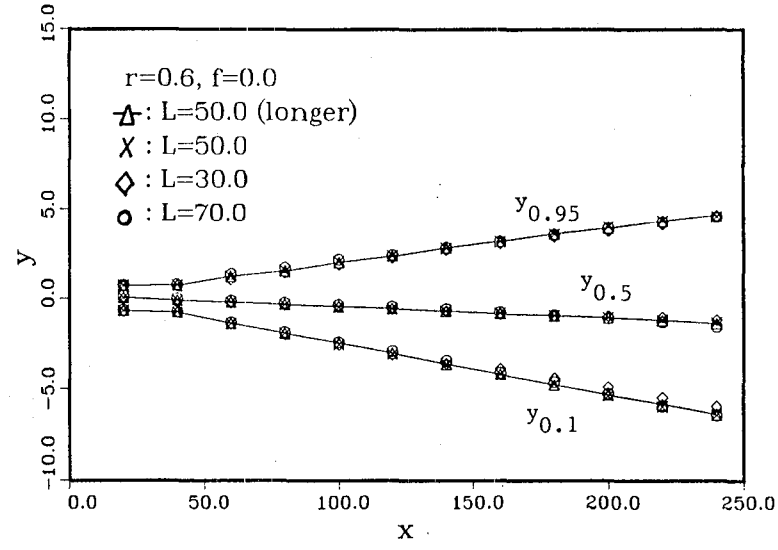

Fig.22. Effect of L on the growth of a mixing layer for vorticity thickness δ_w and the positions of $y_{0.95}$, $y_{0.5}$, and $y_{0.1}$.

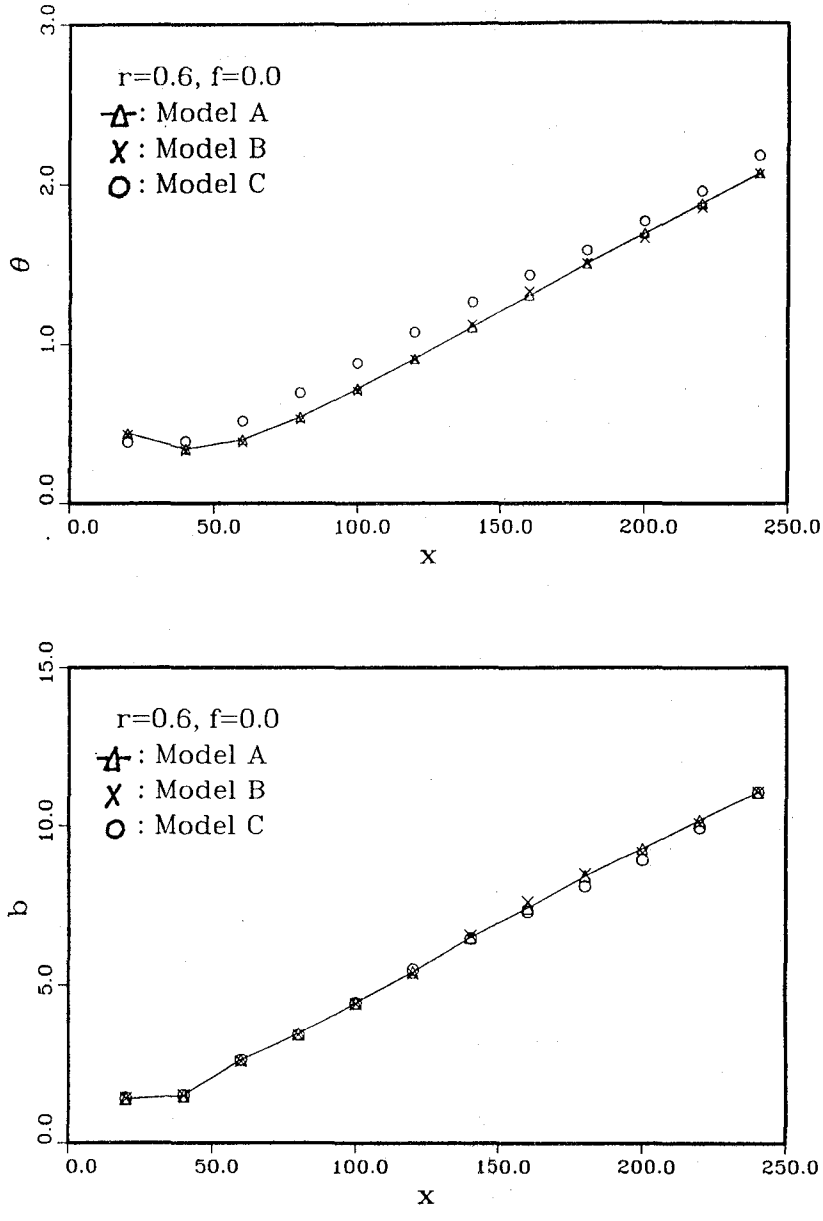

Fig.23. Effect of the difference of the wall models on the growth of a mixing layer for momentum thickness θ and mixing layer thickness b. $L = 50.0$.

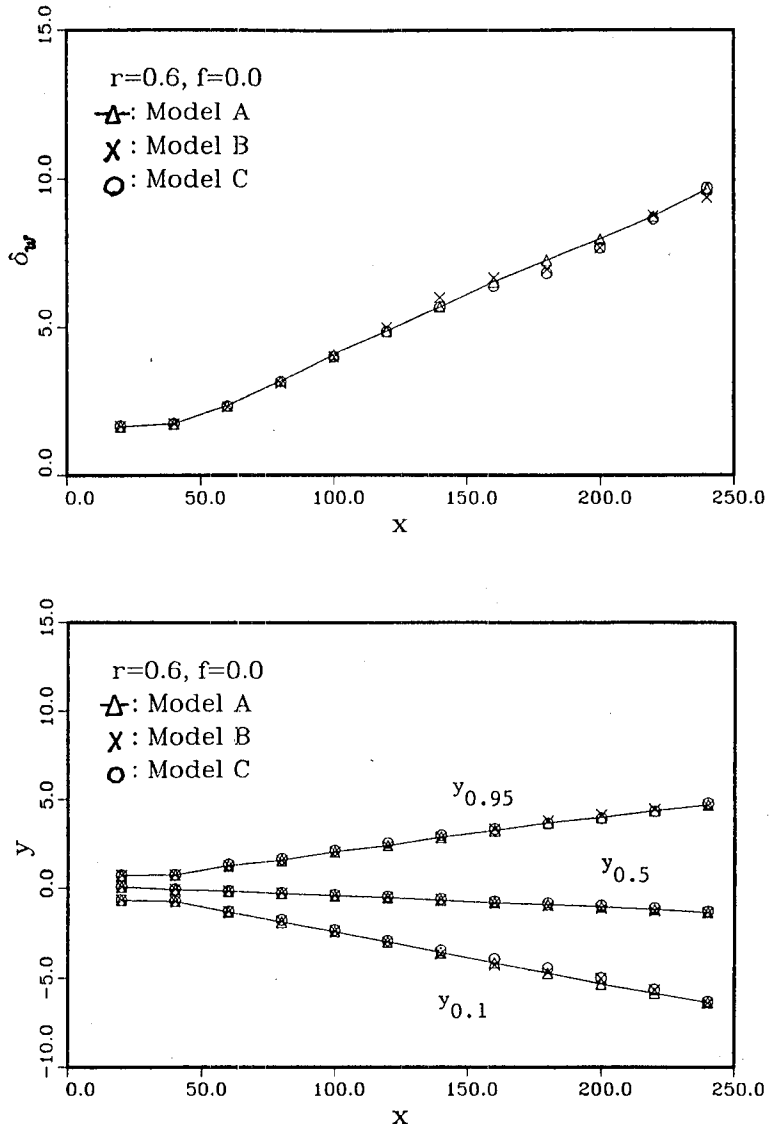

Fig.24. Effect of the difference of the wall models on the growth of a mixing layer for vorticity thickness δ_w and the positions of $y_{0.95}$, $y_{0.5}$, and $y_{0.1}$. $L = 50.0$.

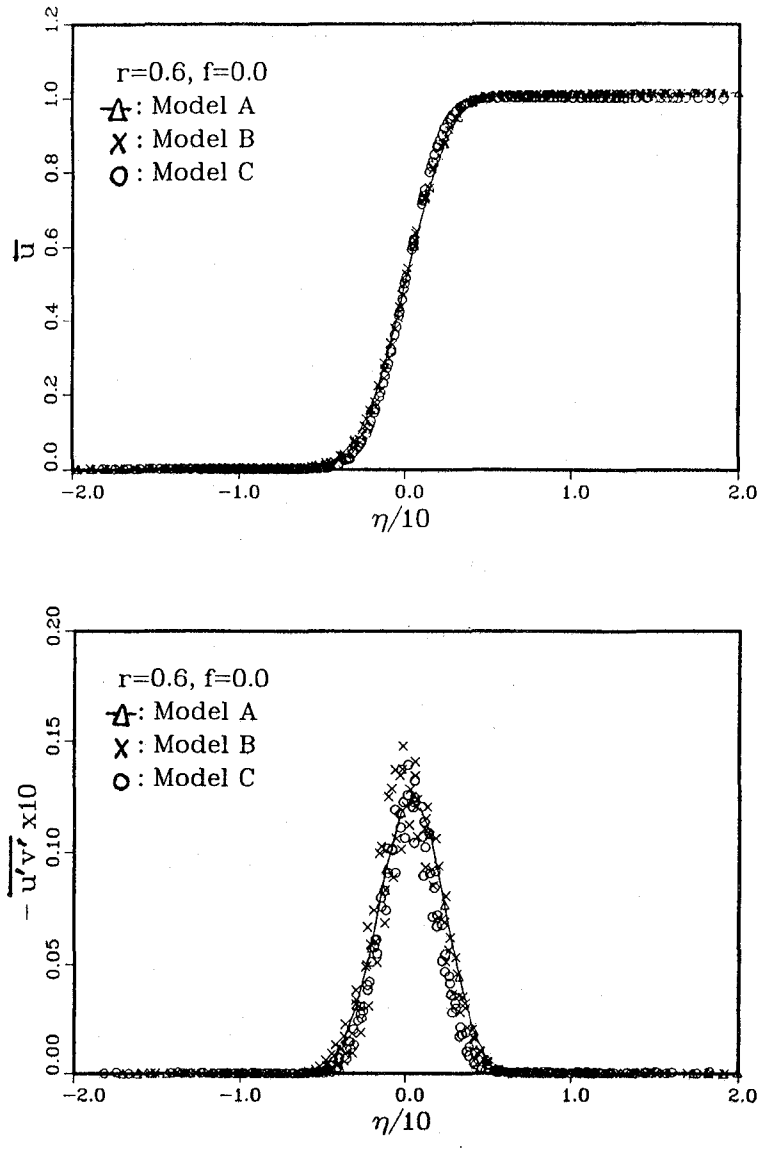

Fig.25 . Effect of the difference of the wall models on $\bar{u}$ and $-\overline{u'v'}$. L = 50.0. x=120, 140 160, 180, and 200.

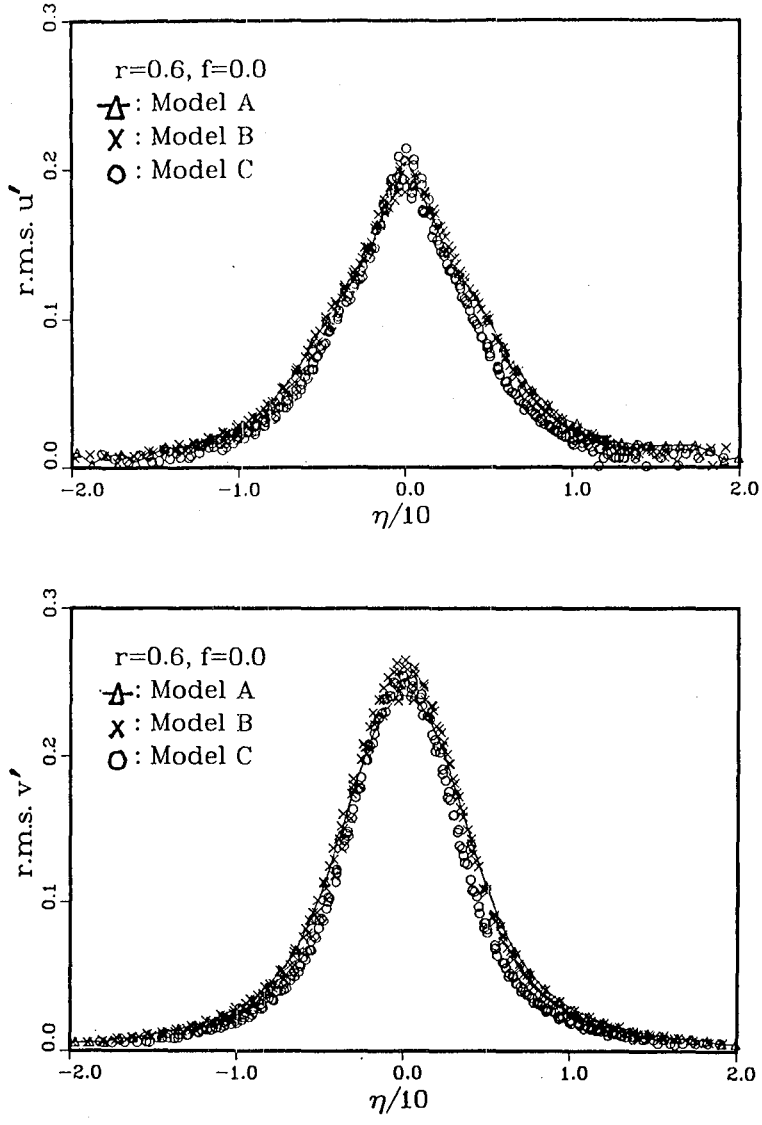

Fig.26 . Effect of the difference of the wall models on *r.m.s.* u' and *r.m.s.* v'. $L = 50.0$. x=120, 140, 160, 180, and 200.

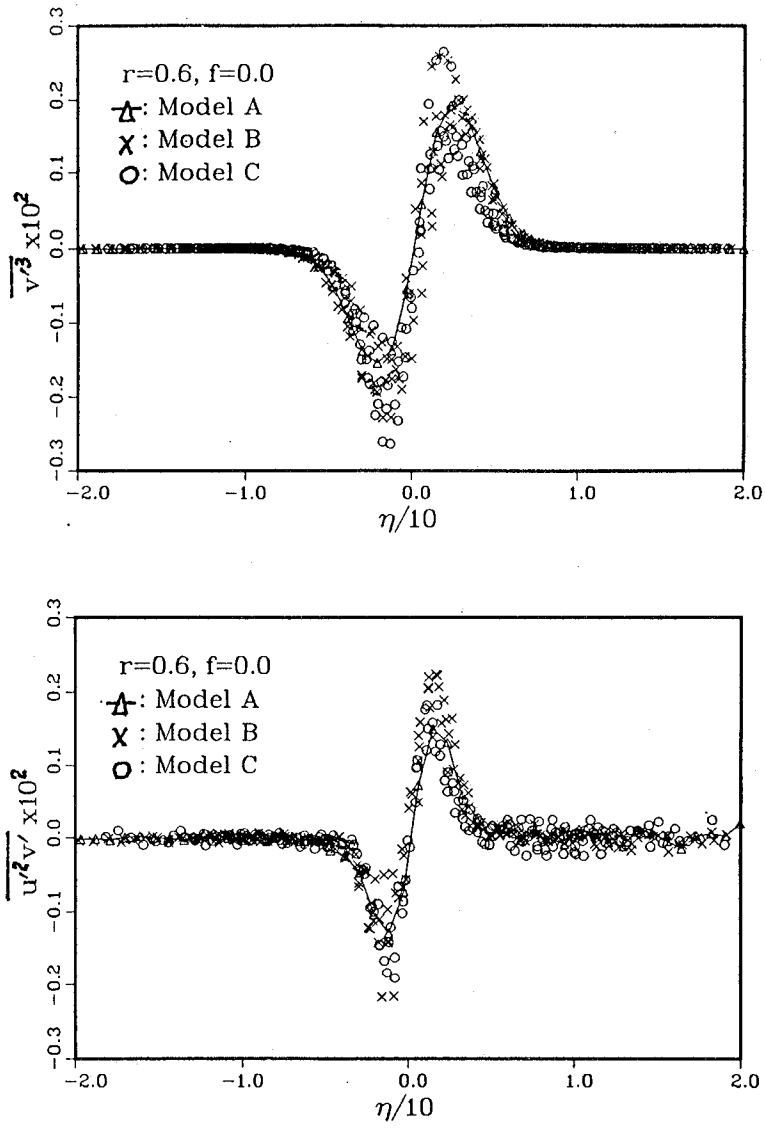

Fig.27 . Effect of the difference of the wall model on $\overline{v'^3}$ and $\overline{u'^2v'}$. L = 50.0. x=120, 140, 160, 180, and 200.

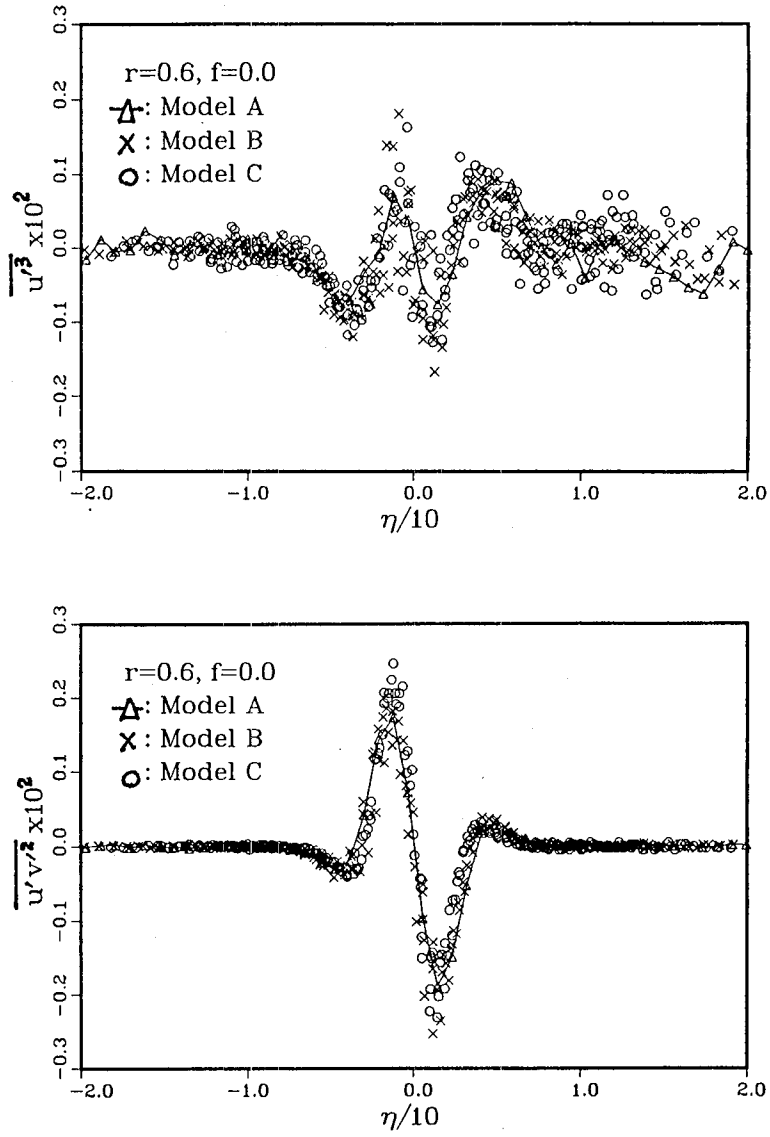

Fig.28 . Effect of the difference of the wall model on $\overline{u\prime^3}$ and $\overline{u'v\prime^2}$. L = 50.0. x=120, 140, 160, 180, and 200.

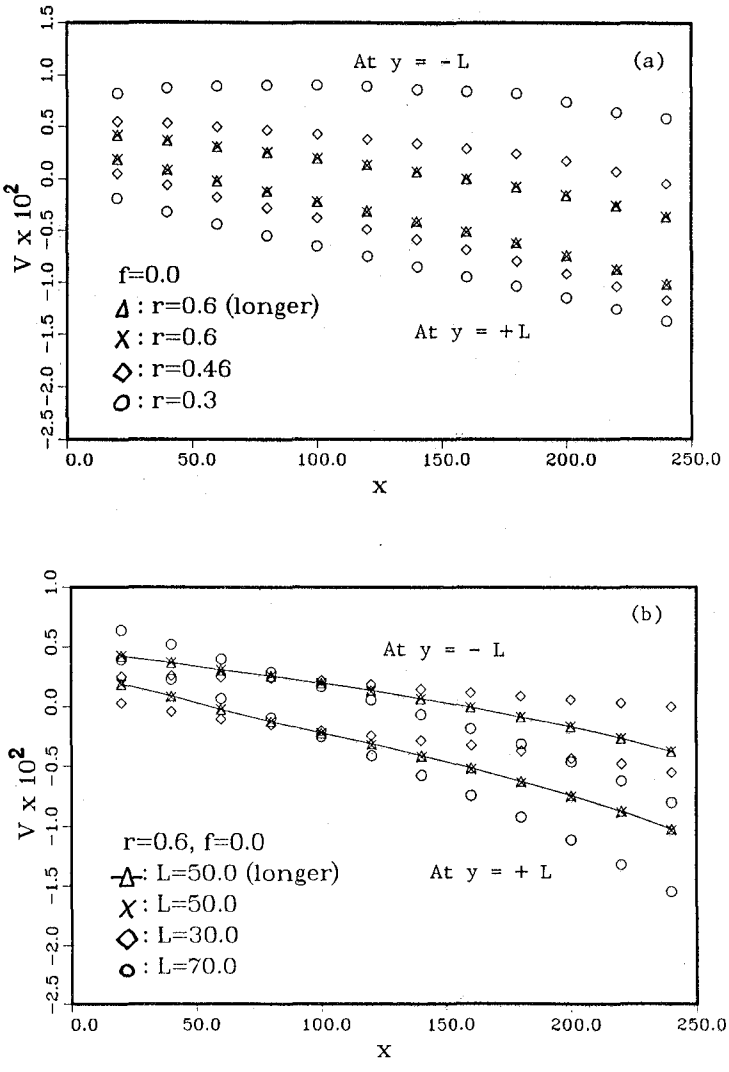

Fig.29. Effect of parameters on the normal velocity V on the walls for Model A. (a) velocity ratio r. $L = 50.0$ (b) half width of a duct L. $r = 0.6$

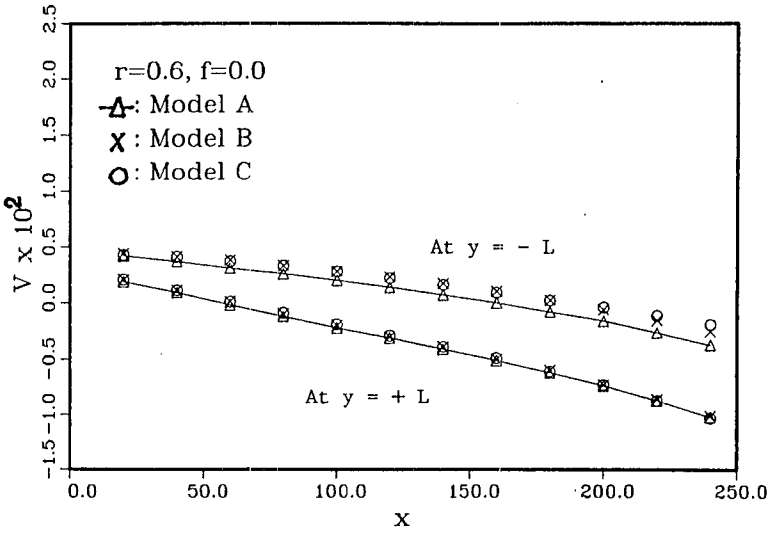

Fig.30. Effect of the difference of the wall models on the normal velocity V on the walls. $r = 0.6$.

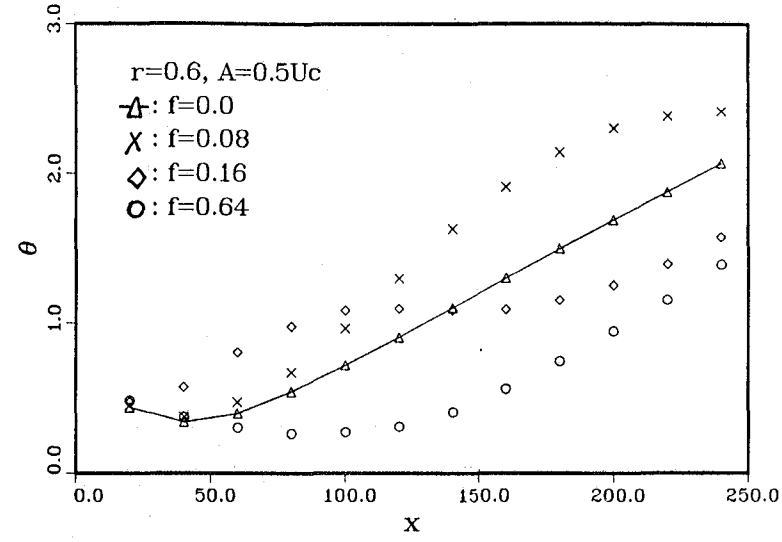

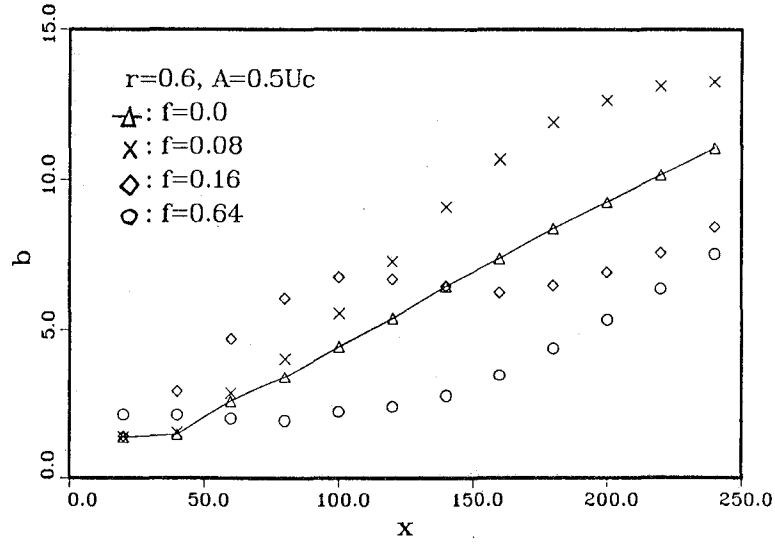

Fig.31. Effect of forcing frequency on the mixing layer thickness for θ and b at $A = 0.5U_c$.

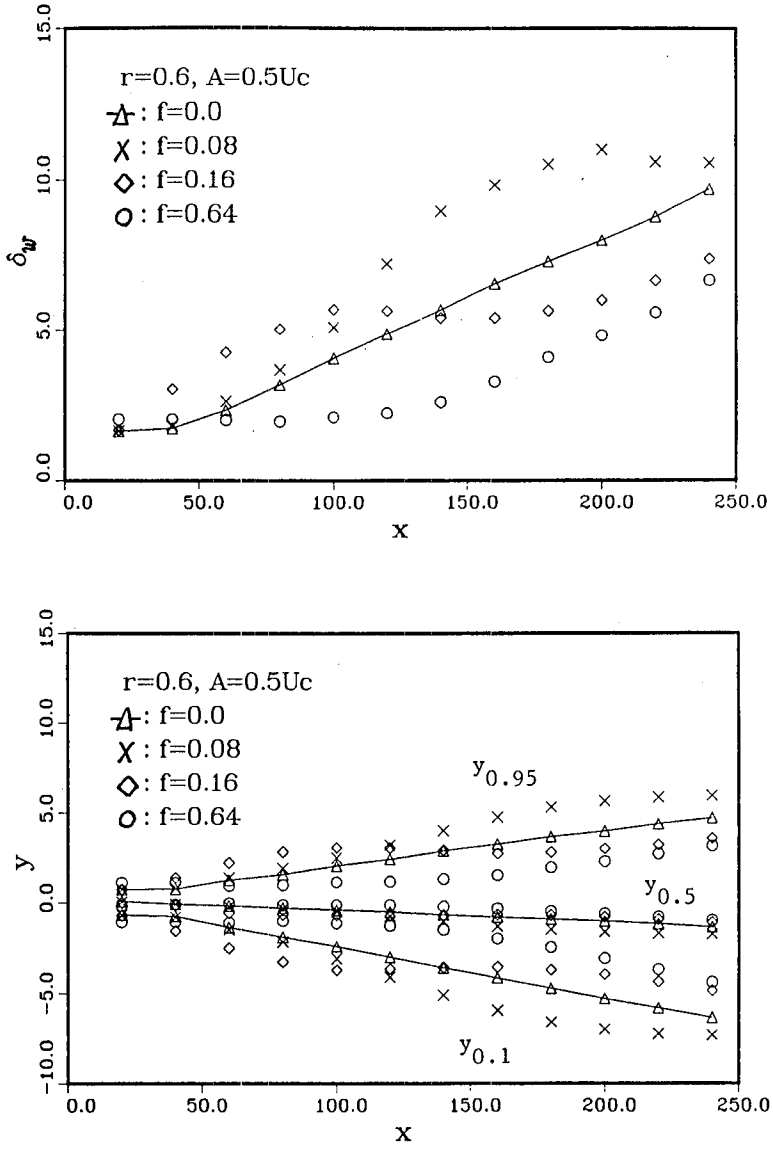

Fig.32. Effect of forcing frequency on the mixing layer thickness for δ_w, $y_{0.95}$, $y_{0.5}$, and $y_{0.1}$ at $A = 0.5U_c$.

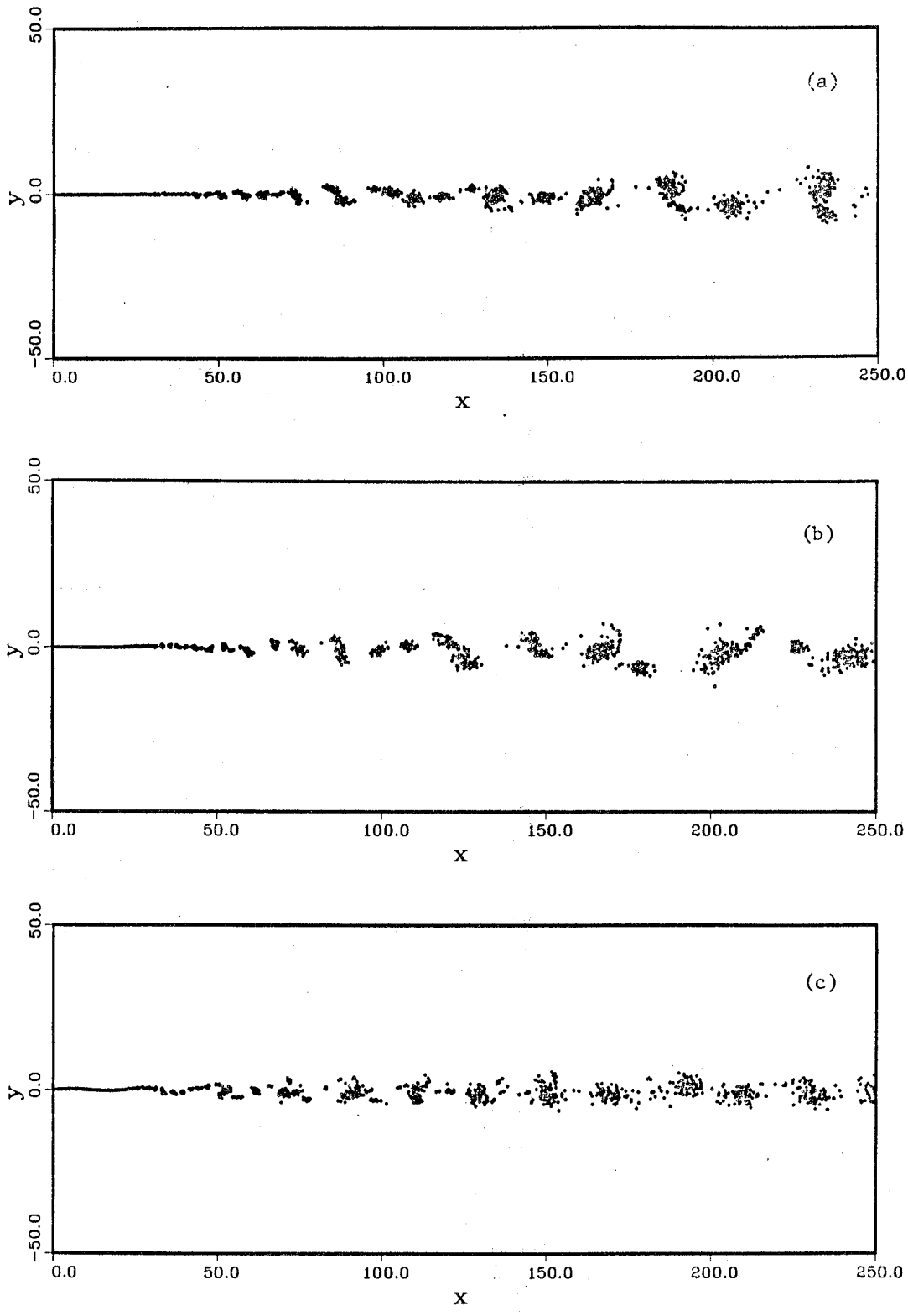

Fig.33. Effect of forcing frequency on a mixing layer at $t = 1000.0$ and $A = 0.5U_c$. (a) $f = 0.0$ (unforced), (b) $f = 0.08(= f_p/4)$, (c) $f = 0.16(= f_p/2)$

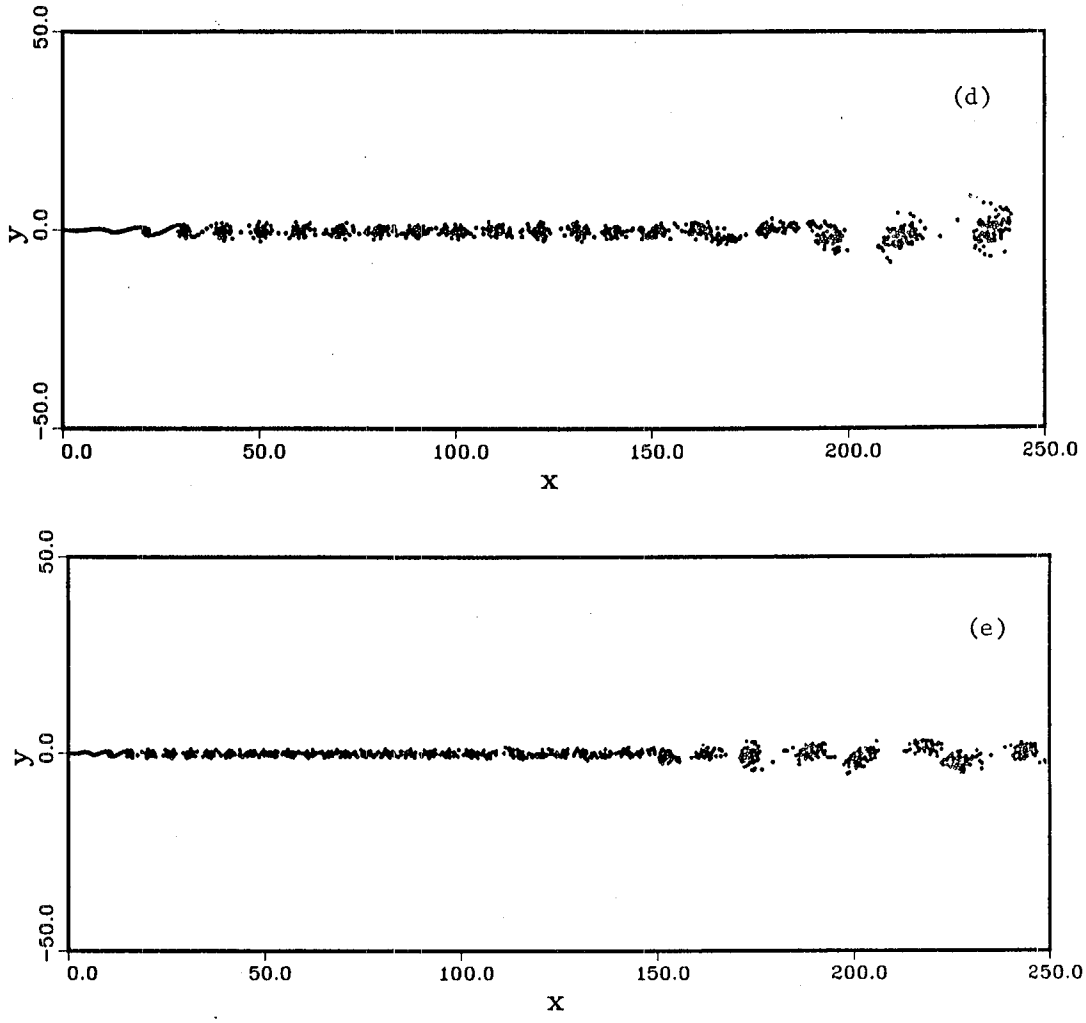

Fig.33.-continued. (d) $f = 0.32(= f_p)$, (e) $f = 0.64(= 2f_p)$

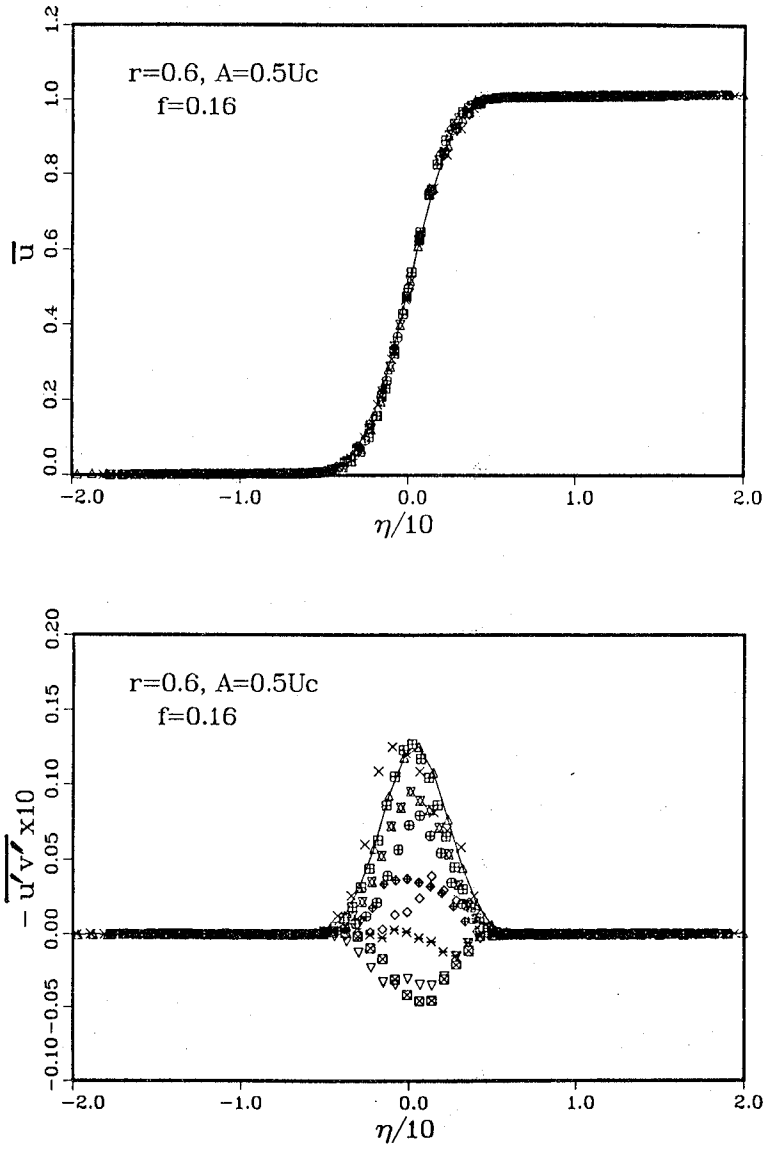

Fig.34. Profiles of the mean velocity $\bar{u}$ and the Reynolds stress $-\overline{u'v'}$ in a low-frequency forced mixing layer at $r = 0.6$, $A = 0.5U_c$, $f = 0.16$. ✗ :x=80, ◇ :x=100, ▽ :x=120, ⊠ :x=140, ✳ :x=160, ⊕ :x=200, ⊠ :x=220, ⊞ :x=240. —△— : unforced

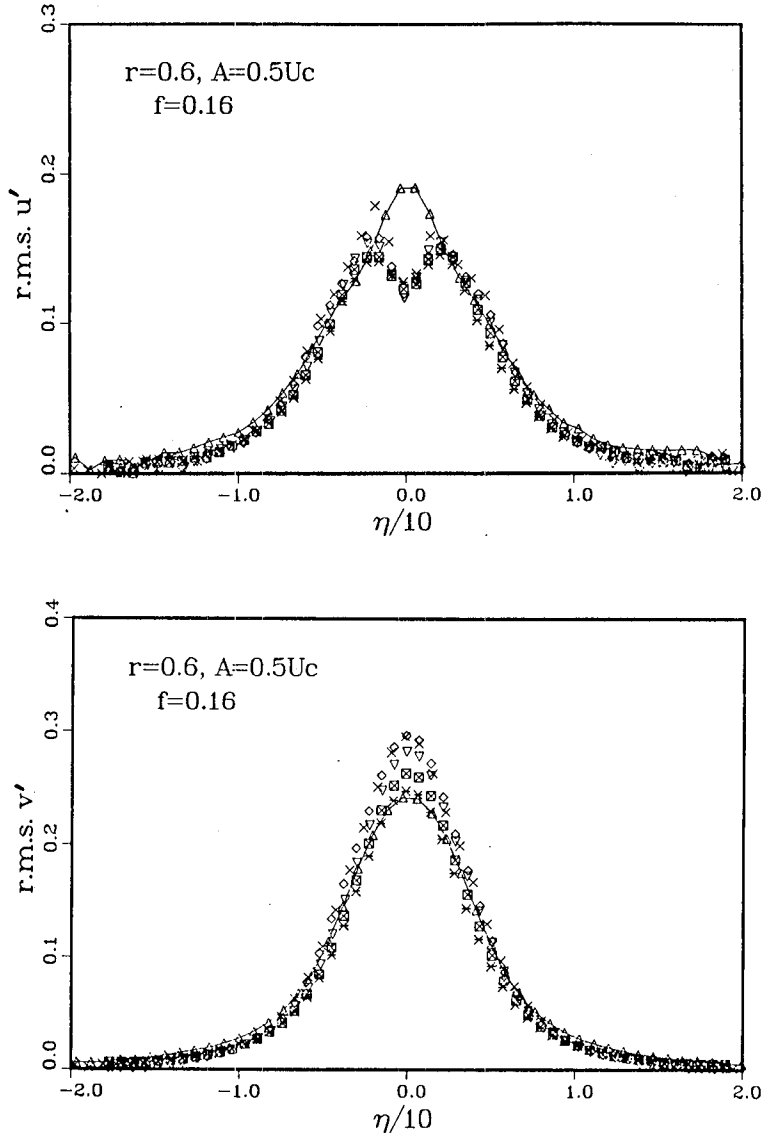

Fig.35. Profiles of *r.m.s.* u' and *r.m.s.* v' in Region II in a low-frequency forced mixing layer at r=0.6, $A = 0.5U_c$, and f=0.16. (For legend, see Fig.34)

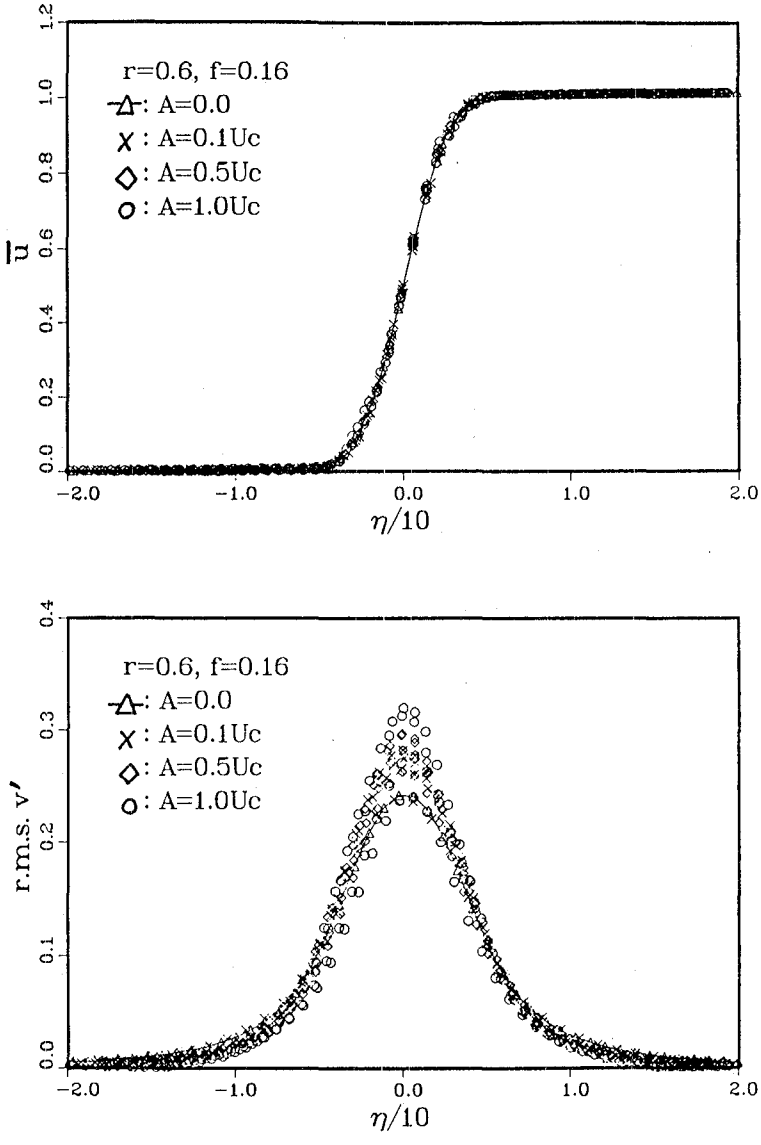

Fig.36. Effect of forcing amplitude on $\bar{u}$ and $r.m.s.\ v'$.

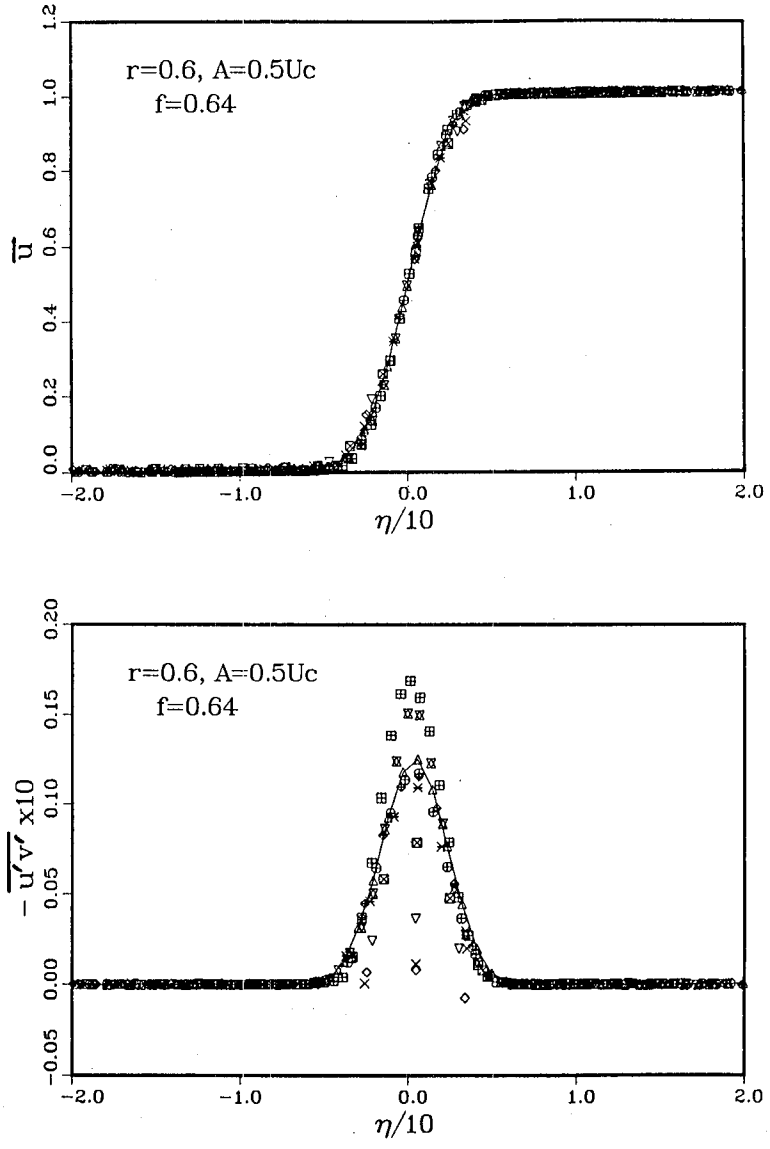

Fig.37. Profiles of $\bar{u}$ and $-\overline{u'v'}$ in a high-frequency forced mixing layer at r=0.6, A = $0.5U_c$, and f=0.64. ✕ :x=80, ◇ :x=100, ▽ :x=120, ⊠ :x=140, ✳ :x=160, ⊕ :x=180. ⊕ :x=200, ⊠ :x=220, ⊞ :x=240. —△— : unforced

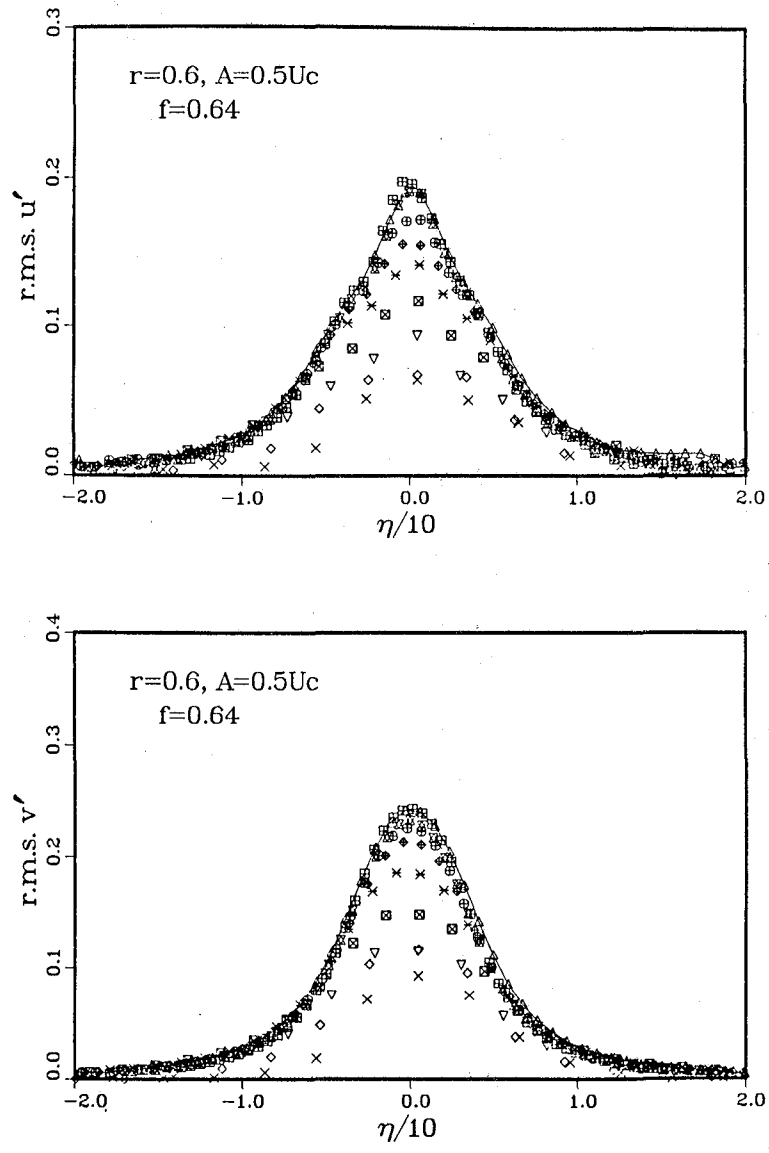

Fig.38. Profiles of *r.m.s.* u' and *r.m.s.* v' in a high-frequency forced mixing layer at r=0.6, $A = 0.5U_c$. and f=0.64. (For legend, see Fig.37.)

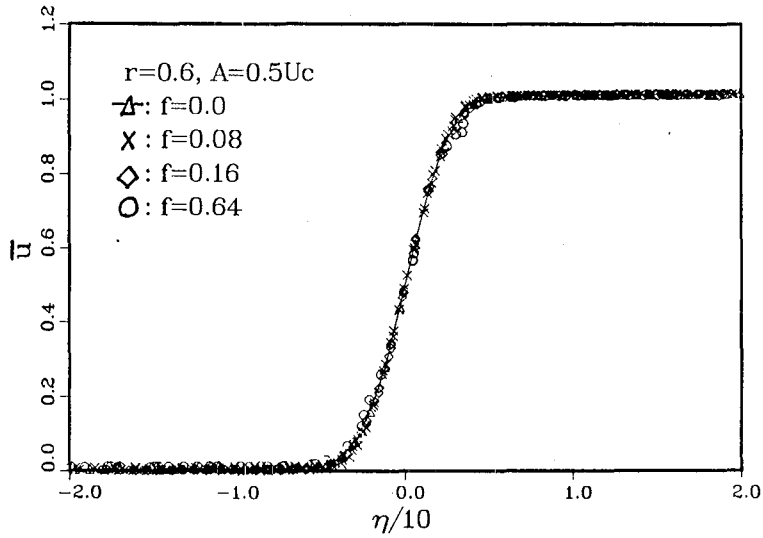

Fig.39. Effect of forcing frequency on the mean velocity $\bar{u}$ at r=0.6, and $A = 0.5U_c$. x=80, 100, 120, 140, 160, 180, and 200.

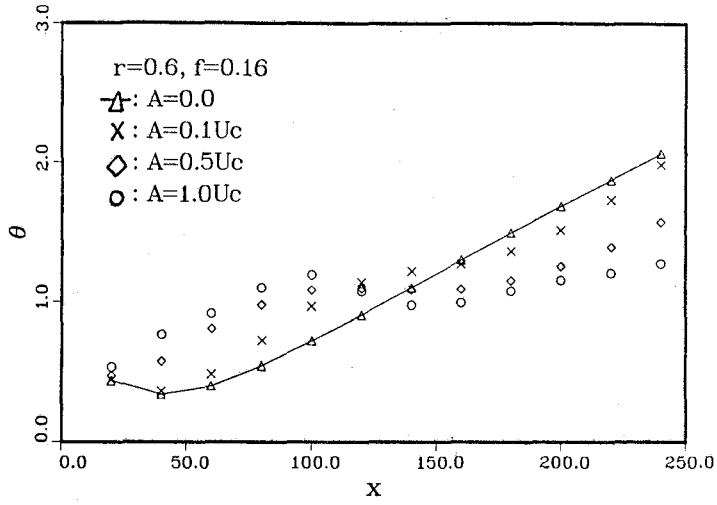

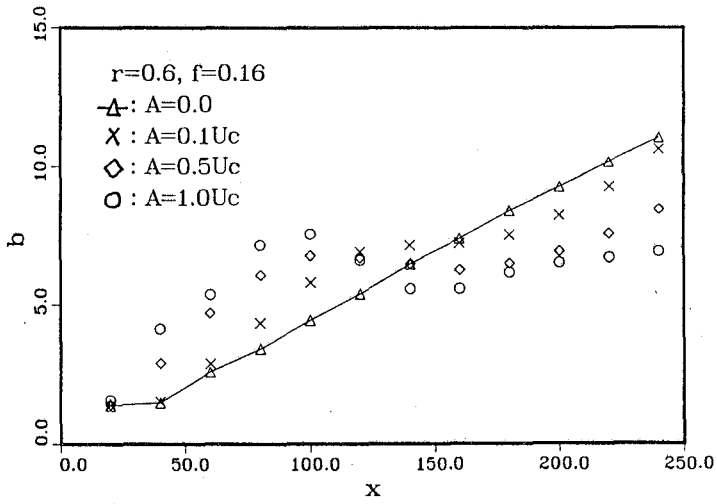

Fig.40. Effect of forcing amplitude on θ and b.

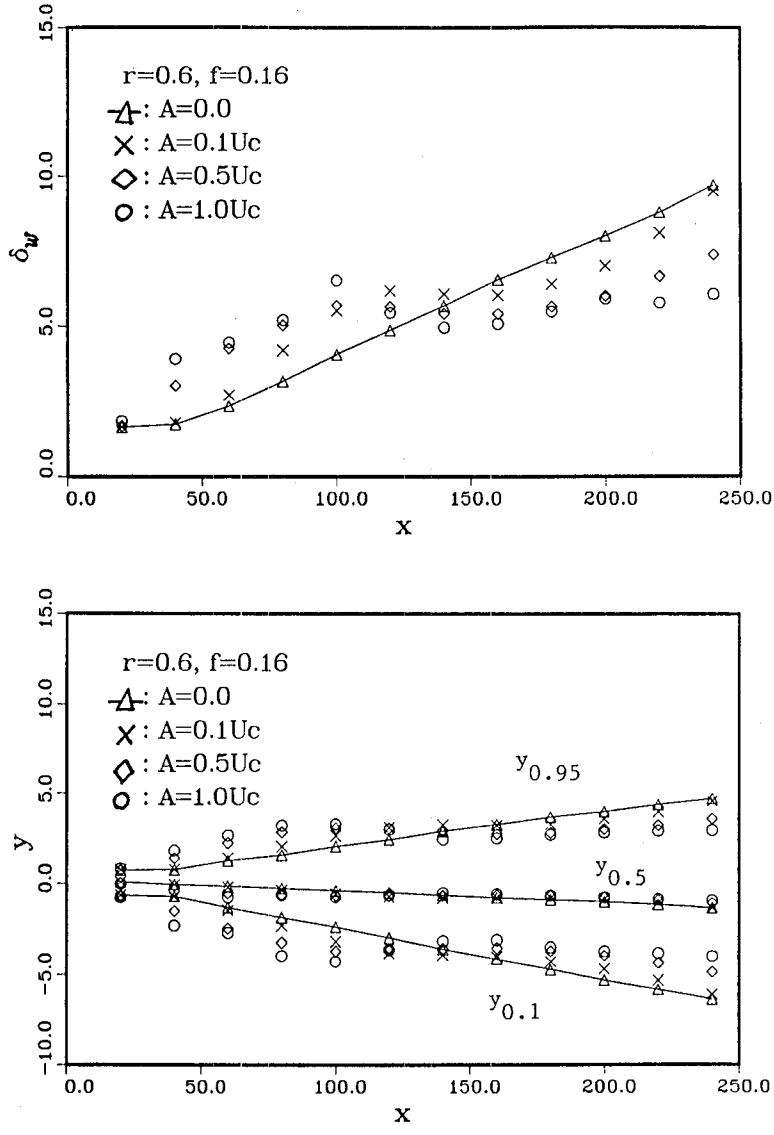

Fig.41. Effect of forcing amplitude on δ_w, $y_{0.95}$, $y_{0.5}$, and $y_{0.1}$.

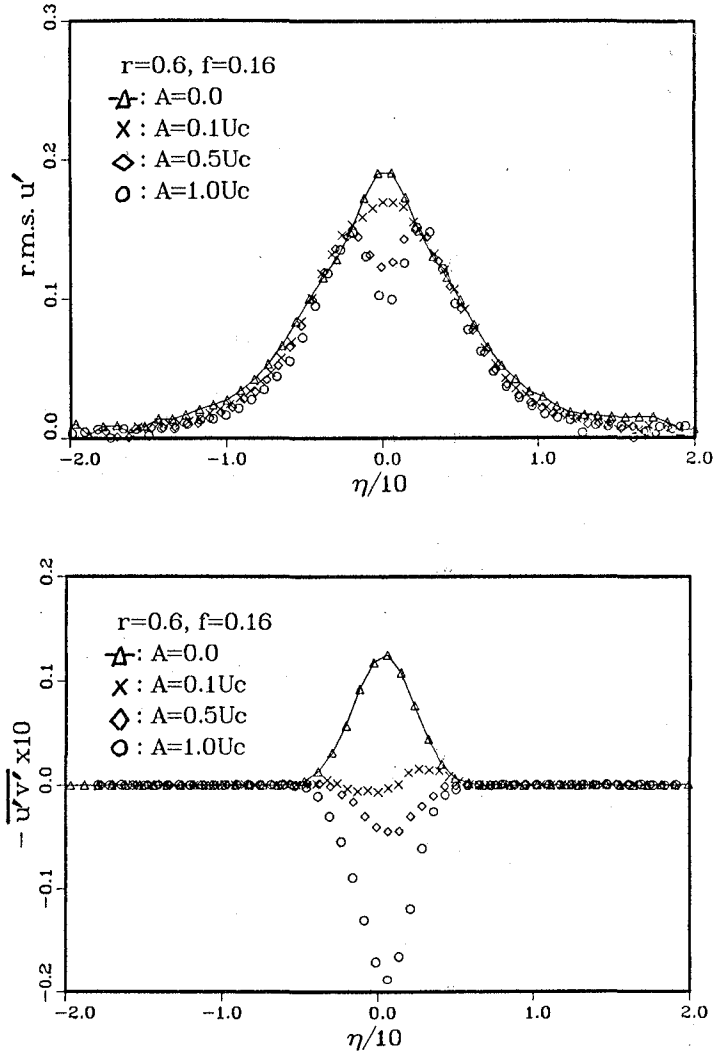

Fig.42. Effect of forcing amplitude on $r.m.s.\ u'$ and $-\overline{u'v'}$ in Region II. x=140.

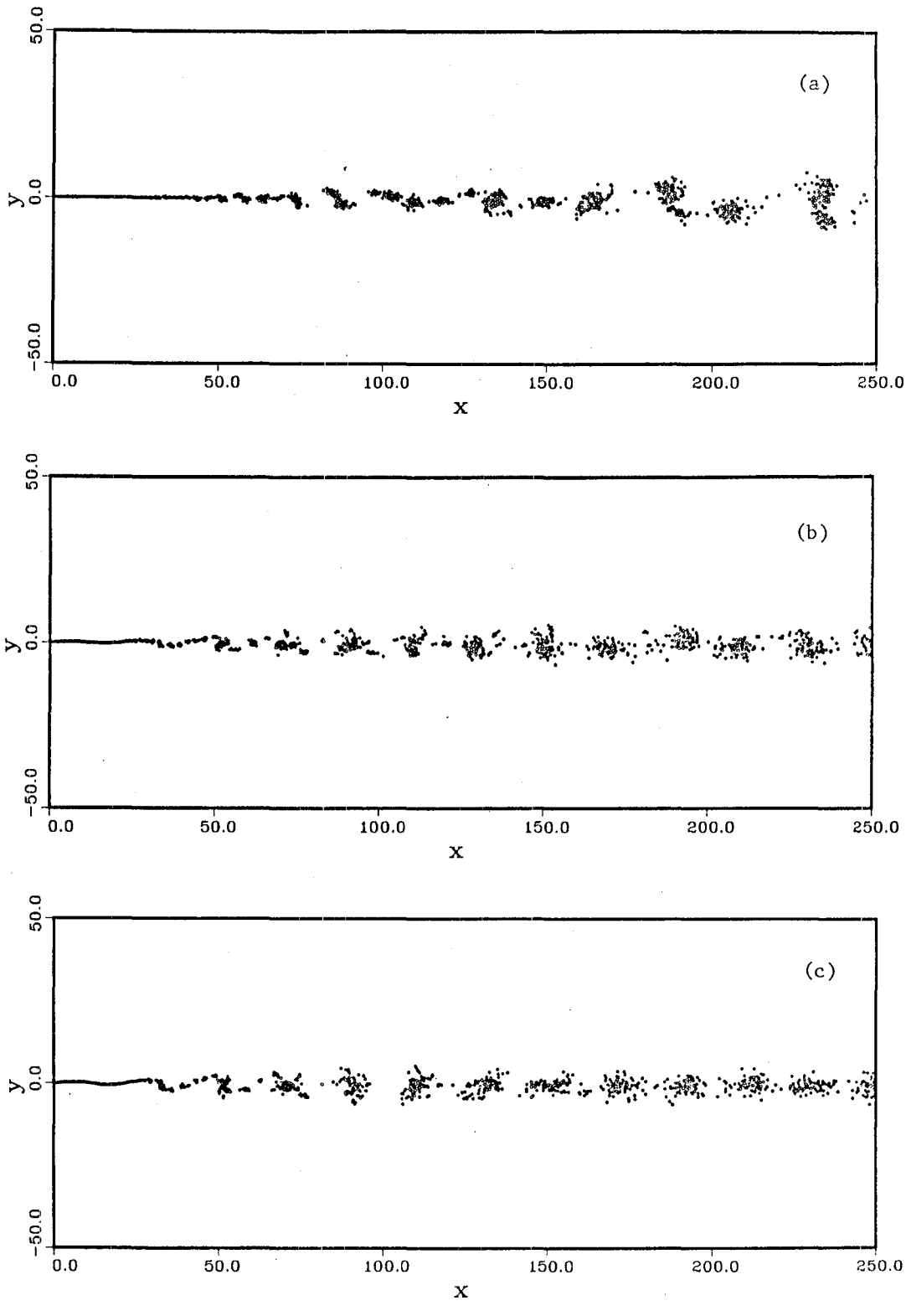

Fig.43. Effect of forcing amplitude on a mixing layer at $t = 1000.0$. $f = 0.16$. (a) $A = 0.0$ (unforced), (b) $A = 0.5U_c$, (c) $A = U_c$

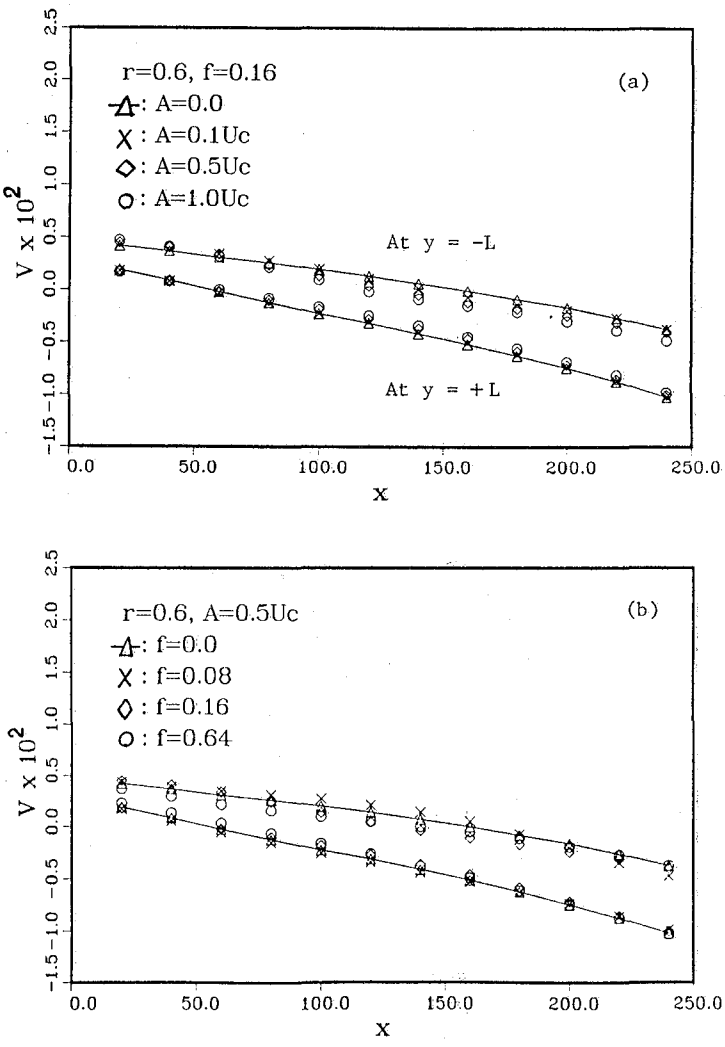

Fig.44. Effect of forcing on the normal velocity on the walls at $r = 0.6$ and $L = 50.0$. (a) effect of forcing amplitude at $f = 0.16$ (b) effect of forcing frequency for $A = 0.5U_c$.

1. Report No.	2. Government Accession No.	3. Recipient's Catalog No.
NASA TM-88235		

4. Title and Subtitle	5. Report Date
VORTEX SIMULATION OF FORCED MIXING LAYERS	June 1986
	6. Performing Organization Code

7. Author(s)	8. Performing Organization Report No.
Osamu Inoue and Anthony Leonard*	A-86191
	10. Work Unit No.

9. Performing Organization Name and Address	11. Contract or Grant No.
Ames Research Center Moffett Field, CA 94035	

12. Sponsoring Agency Name and Address	13. Type of Report and Period Covered
National Aeronautics and Space Administration Washington, DC 20546	Technical Memorandum
	14. Sponsoring Agency Code
	505-60-21

15. Supplementary Notes *NRC Research Associate.

Point of Contact: Osamu Inoue, Ames Research Center, MS 202A-1,
Moffett Field, CA 94035 (415) 694-6667 or FTS 464-6667

16. Abstract

Two-dimensional, spatially growing, turbulent mixing layers are simulated numerically by a vortex method and the results are compared with those determined experimentally. The effects of artificial forcing on flow development are also studied. Many of the flow features which have been observed experimentally are reproduced, and good quantitative agreements between experiments and computations are obtained.

17. Key Words (Suggested by Author(s))	18. Distribution Statement
Turbulence Mixing layers Vortex method	Unlimited Subject category - 02

19. Security Classif. (of this report)	20. Security Classif. (of this page)	21. No. of Pages	22. Price*
Unclassified	Unclassified	71	A04

*For sale by the National Technical Information Service, Springfield, Virginia 22161

End of Document